To the Graduate Council:

I am submitting herewith a thesis written by Robert Paul Roy entitled "Evaluation of Head Linear and Rotational Acceleration Response to Various Linear-Induced Impact Scenarios." I have examined the final electronic copy of this thesis for form and content and recommend that it be accepted in partial fulfillment of the requirements for the degree of Master of Science, with a major in Engineering Science.

James Evans Lyne
Major Professor

We have read this thesis
and recommend its acceptance:

Tyler Kress

John Landes

Accepted for the Council:

Carolyn R. Hodges
Vice Provost and Dean of the
Graduate School

(Original signatures are on file with official student records)

EVALUATION OF HEAD LINEAR AND ROTATIONAL ACCELERATION RESPONSE TO VARIOUS LINEAR-INDUCED IMPACT SCENARIOS

A Thesis Presented for the
Master of Science Degree
The University of Tennessee, Knoxville

Robert Paul Roy
December 2007

Copyright © 2007 by Robert Paul Roy
All rights reserved.

DEDICATION

I dedicate this to my parents, Paul and Deborah, and my sisters, Beth and Joy. Without their support and encouragement over the years, I would not have made it this far.

ACKNOWLEDGEMENTS

First, I would like to thank Dave Halstead for the opportunity to work on this project and the Protective Headgear Manufacturers' Association (PHMA) for financing this research. In addition, I would like to express my thanks to Mel Cook, Laura Ziegler, and everyone at Southern Impact Research Center for the support, assistance, and guidance they have offered to me not only on this project, but over the past several years. Finally, I would like to thank Dr. Evans Lyne, Dr. Tyler Kress, and Dr. John Landes for taking the time to serve as my committee.

ABSTRACT

Incidents resulting in head injury generally involve components of both linear and rotational motion. The protection of the head from injury most often comes from the use of some form of helmet. Helmets currently are designed only to protect the head from linear accelerations. Recent research involving the analysis of concussion in professional football suggested that linear accelerations are more consistent in the prediction of concussion, with the resultant rotational accelerations correlating to the peak linear accelerations of the impact.

This research proposes to determine if the situation of the head impact has an effect on the correlation of the linear and rotational accelerations, as well as to determine if the linear acceleration is consistent as the predominating factor of concussion in various linear-induced impact scenarios. Through the development of various impact test conditions using bicycle helmets on a biofidelic test headform and Hybrid III neck, it was determined that the correlation between the linear and rotational accelerations experienced by the head is affected in part by the impact situation. Additionally, while linear accelerations may be adequate predictors of concussion in some impact scenarios, it was determined that there are situations in which the rotational accelerations would be the more dominating factor in the expected probability of concussion.

TABLE OF CONTENTS

CHAPTER 1

Introduction **1**

CHAPTER 2

Background **3**

2.1 Mechanisms of Head Injury 3

2.2 Principles of Head Protection 6

2.3 Rotational Acceleration of the Head 9

2.4 NFL Study on MTBI 11

CHAPTER 3

Experiment Objective, Setup, and Procedure **13**

3.1 Objective of Experiment 13

3.2 Description of Equipment 14

3.3 Test Procedure 18

CHAPTER 4

Results **23**

CHAPTER 5

Conclusions & Recommendations **33**

References **35**

Appendix A

RAW DATA **39**

Appendix B

HIGH-SPEED VIDEO **53**

Appendix C

MISCELLANEOUS INFORMATION **66**

LIST OF TABLES

Table 2.1 - MTBI thresholds developed by Zhang, et al (34) and Newman, et al (24) 11
Table 3.1 - Target velocities for specified energy levels used in test conditions.....18
Table 4.1 - t-test results at 95% confidence level 32
Table 4.2 – Standard deviations and true mean values of helmets X and Y 32
Table A.1 - Raw data sorted by target energy level 40
Table C.1 - Information on Endevco 7264B-2000 Piezoresistive Accelerometers.....67

LIST OF FIGURES

Figure 3.1 - (a) Modified NOCSAE test headform with Hybrid III neck, and (b) 3-2-2-2 configuration of accelerometers on headform mounting block....14
Figure 3.2 - View of Drop Tower System....15
Figure 3.3 - Linear impactor system with (a) view of head/neck assembly and end of ram, and (b) compressed air tank with control panel....16
Figure 3.4 - Drawing of Linear Impactor System from NOCSAE (20)....17
Figure 3.5 - View of test headform and flat anvil in Condition 1....19
Figure 3.6 - View of setup for Condition 2....19
Figure 3.7 - View of test setup for Condition 3....20
Figure 3.8 - View of head and impactor ram in Condition 4....20
Figure 3.9 – Arrow shows impact test line....22
Figure 4.1 – Average of linear accelerations of locations A and B with concussion probability limits....24
Figure 4.2 - Average rotational accelerations of locations A and B with concussion probability limits....24
Figure 4.3 - Average SI of locations A and B with concussion probability limits....25
Figure 4.4 - Average HIC of locations A and B with concussion probability limits....25
Figure 4.5 - Average GAMBIT of locations A and B with concussion probability limits....26
Figure 4.6 - Average maximum HIP of locations A and B with concussion probability limits....26
Figure 4.7 - Linear acceleration versus rotational acceleration per test condition....28
Figure 4.8 - Linear acceleration versus rotational acceleration in Condition 1....29
Figure 4.9 - Linear acceleration versus rotational acceleration in Condition 2....29
Figure 4.10 - Linear acceleration versus rotational acceleration in Condition 3....30
Figure 4.11 - Linear acceleration versus rotational acceleration in Condition 4....30
Figure A.1 - Linear acceleration time trace for Condition 1 at 77 Joules....41
Figure A.2 - Linear acceleration time trace for Condition 1 at 121 Joules....41
Figure A.3 - Linear acceleration time trace for Condition 1 at 160 Joules....42

Figure A.4 - Linear acceleration time trace for Condition 2 at 77 Joules 42
Figure A.5 - Linear acceleration time trace for Condition 2 at 121 Joules 43
Figure A.6 - Linear acceleration time trace for Condition 2 at 160 Joules 43
Figure A.7 - Linear acceleration time trace for Condition 3 at 77 Joules 44
Figure A.8 - Linear acceleration time trace for Condition 3 at 121 Joules 44
Figure A.9 - Linear acceleration time trace for Condition 3 at 160 Joules 45
Figure A.10 - Linear acceleration time trace for Condition 4 at 77 Joules 45
Figure A.11 - Linear acceleration time trace for Condition 4 at 121 Joules 46
Figure A.12 - Linear acceleration time trace for Condition 4 at 160 Joules 46
Figure A.13 - Rotational acceleration time trace for Condition 1 at 77 Joules 47
Figure A.14 - Rotational acceleration time trace for Condition 1 at 121 Joules 47
Figure A.15 - Rotational acceleration time trace for Condition 1 at 160 Joules 48
Figure A.16 - Rotational acceleration time trace for Condition 2 at 77 Joules 48
Figure A.17 - Rotational acceleration time trace for Condition 2 at 121 Joules 49
Figure A.18 - Rotational acceleration time trace for Condition 2 at 160 Joules 49
Figure A.19 - Rotational acceleration time trace for Condition 3 at 77 Joules 50
Figure A.20 - Rotational acceleration time trace for Condition 3 at 121 Joules 50
Figure A.21 - Rotational acceleration time trace for Condition 3 at 160 Joules 51
Figure A.22 - Rotational acceleration time trace for Condition 4 at 77 Joules 51
Figure A.23 - Rotational acceleration time trace for Condition 4 at 121 Joules 52
Figure A.24 - Rotational acceleration time trace for Condition 4 at 160 Joules 52
Figure B.1 - High-speed video screen captures of Condition 1 at 77 Joules.....54
Figure B.2 - High-speed video screen captures of Condition 1 at 121 Joules.....55
Figure B.3 - High-speed video screen captures of Condition 1 at 160 Joules.....56
Figure B.4 - High-speed video screen captures of Condition 2 at 77 Joules.....57
Figure B.5 - High-speed video screen captures of Condition 2 at 121 Joules.....58
Figure B.6 - High-speed video screen captures of Condition 2 at 160 Joules.....59
Figure B.7 - High-speed video screen captures of Condition 3 at 77 Joules.....60
Figure B.8 - High-speed video screen captures of Condition 3 at 121 Joules.....61
Figure B.9 - High-speed video screen captures of Condition 3 at 160 Joules.....62
Figure B.10 - High-speed video screen captures of Condition 4 at 77 Joules.....63

Figure B.11 - High-speed video screen captures of Condition 4 at 121 Joules 64
Figure B.12 - High-speed video screen captures of Condition 4 at 160 Joules 65
Figure C.1 - View of DC Differential Voltage Amplifier and Connector Box.....67
Figure C.2 - Endevco 7264B acclerometer data sheet (page 1).....68
Figure C.3 - Endevco 7264B acclerometer data sheet (page 2).....69
Figure C.4 - Endevco model 136 voltage amplifier data sheet (page 1).....70
Figure C.5 - Endevco model 136 voltage amplifier data sheet (page 2).....71
Figure C.6 - National Instruments 6024E data acquisition card data sheet (page 1) 72
Figure C.7 - National Instruments 6024E data acquisition card data sheet (page 2) 73
Figure C.8 - Sample of output screen from BIODAQ software 74
Figure C.9 - Sample of filtered data screen from BIODAQ software 75

NOMENCLATURE

a – linear acceleration

a_X – linear acceleration in the x-direction

a_Y – linear acceleration in the y-direction

a_Z – linear acceleration in the z-direction

CG – center of gravity

df – degrees of freedom

g – acceleration due to gravity (9.81 m/s^2)

G(t) – GAMBIT function

KE – kinetic energy

m – mass

n – number of samples

p-value – statistical probability value

R – correlation coefficient

R^2 – coefficient of determination

S_X – standard deviation

t – time

t-value – value from t-test

v – velocity

$\bar{x}$ – sample mean value

X – denotation for test helmet manufacturer (made with EPS)

Y – denotation for test helmet manufacturer (made with EPU)

α – rotational acceleration

α_X – rotational acceleration about the x-axis

α_Y – rotational acceleration about the y-axis

α_Z – rotational acceleration about the z-axis

ABBREVIATIONS

ASTM – American Society for Testing and Materials

BIODAQ – data acquisition testing software developed by Biokinetics and Associates Ltd.

CPSC – Consumer Product Safety Commission

DAI – diffuse axonal injury

DBI – diffuse brain injury

EPS – expanded polystyrene

EPU – expanded polyurethane

GAMBIT – Generalized Acceleration Model for Brain Injury Threshold

HIC – Head Injury Criterion

HIC_{15} – Head Injury Criterion evaluated over 15 ms time interval

HIP – Head Impact Power

HIP_m – maximum Head Impact Power

HPI – head positioning index

MTBI – mild traumatic brain injury

NOCSAE – National Operating Committee on Standards for Athletic Equipment

NFL – National Football League

SI – Gadd Severity Index

TBI – traumatic brain injury

- CHAPTER 1 -

INTRODUCTION

When it comes to injuries or trauma to the head and brain, important factors to consider are the acceleration and motion experienced by the head (6, 9, 10, 15, 22). There are two types of motion that must be considered: linear (or translational) motion and rotational (or angular) motion and the accelerations associated with each (9, 10, 15, 26). Helmets are used to help reduce the risk of head injuries, but are primarily designed to protect the head against linear forces, and not the rotational motions that may result (14, 15, 22). The issue of rotational acceleration as an important factor in head injury has been acknowledged for some time (2, 6, 7, 9, 10, 13), but the role of helmets in mitigating rotational accelerations is not examined in existing standards (14, 15, 22, 28). Current helmet standards rely solely on their performance in cases of linear motion and utilize failure criteria in the assessment of head injury that are functions of the linear accelerations, with no regard for any rotational effects (7, 14, 15). While there have been some head injury functions developed where the rotational aspects are taken into account (21, 27), they are not required for assessment in current standards (14, 15, 22).

Due to helmets having to satisfy only linear requirements (14, 15, 22), there has been some concern that the focus of helmet design has been adjusted to improve performance in linear situations (such as by increasing the stiffness). So in some situations helmets may not be working as well as they could to manage all aspects of the impact (15). As a result, the increased stiffness may have implications in mild traumatic brain injury (MTBI) (12). For example, there may be two cases in which there is similar visible minor mechanical damage done to identical helmets and identical locations (indicating comparable impact energies), but one person may have virtually no negative after-effects of the impact, while the other person has suffered a severe brain injury. The visible damage of crush to a helmet liner that comes from a linear impact can often be used to evaluate comparable impact energies in helmets that function through permanent deformation. Therefore, from the above example it could be concluded that there is some aspect occurring in one situation that is not in the other.

This could be a result of the impact scenario, which may have a high rotational acceleration in one situation that is not occurring in the other even though similar linear effects have taken place. Confounding this is the wide range of human tolerance to both linear and rotational impacts (12, 18).

It has been believed that rotational acceleration, whether alone or in conjunction with linear acceleration, is a strong influencing factor in injuries sustained to the brain (2, 6, 7, 9, 10, 13, 15, 21, 23, 28). However, there has been some debate as to the true relevance of rotational acceleration when compared with linear acceleration (28, 29). It has been presented that although rotational acceleration may have an effect on the brain, "translational acceleration remains the single most important response to address in future helmet designs" (29). This indicates that there is a direct correlation between linear acceleration and the resultant rotational acceleration in a head impact, so any effects of the rotational motion come as a direct effect of the linear impact. Although this may be true for most instances, this research proposes to determine whether, for different impact scenarios, the relationship between the linear and rotational accelerations results in a direct correlation, or if the relationship between the linear and rotational accelerations are dependent upon the situation of the impact.

- CHAPTER 2 -

BACKGROUND

2.1 Mechanisms of Head Injury

Trauma to the head can be a concern due to the possibility of injury to the brain. Mechanically-induced head injury occurs as a result of "the movement of some part of the head relative to another" (22) that can result in distortion, changes in intracranial pressure, and excessive strains in the brain (2, 3, 7, 9, 10, 22, 26, 34). In general, mechanically-induced brain injuries can be classified as either a MTBI or a traumatic brain injury (TBI), with injuries such as concussion (with or without loss of consciousness) being classified as MTBI while others such as severe diffuse axonal injury (DAI) falling into the TBI category (5, 6, 12, 27). Approximately 80% of brain injuries are classified as MTBI (5), often resulting in the risk of prolonged effects of the MTBI after the initial injury with post-concussion syndrome (3, 5, 11).

Although some injures can easily be classified as either TBI or MTBI there is a large discrepancy separating the two as to where some brain injury can definitely be categorized as one or the other rather than a separation by an easily definable transition region (12). This is compounded by the fact that individual humans have different levels of tolerance. Individual tolerances can be a combined effect of a number of factors, such as age, body/brain mass, etc., such that an injury that would result in a concussion in one person may not have the same effect as on another (11, 18). The brain is also anisotropic, or has different sensitivities to injury when impacted in different locations (12, 18, 27). An additional concern is the apparent increased sensitivity to minor impacts on individuals who have previously sustained a MTBI from which they have not completely recovered (2, 3, 11, 12, 28).

2.1.1 Head Injury Assessment Functions

In addition to the acceleration (such as the peak g) and time duration of impacts that are most often considered, several different assessment functions have been developed for use in the evaluation of head injury. These include the Head Injury Criterion (HIC), the Gadd Severity Index (SI), the Generalized Acceleration Model for Brain Injury Threshold (GAMBIT), and the Head Impact Power (HIP) index (8, 15, 21, 27). The SI and HIC are the most commonly used head injury assessment functions (along with the peak g), particularly in current testing standards, and all are based solely on linear acceleration (14, 15, 24, 27, 34).

The HIC was developed from experimental work, particularly the Wayne State University Cerebral Concussion Tolerance Curve, which was developed from a combination of cadaver skull fracture tests and concussive testing on animals (15, 23, 27, 34). It follows the form

$$HIC = \left[\frac{1}{t_2 - t_1} \int_{t_1}^{t_2} a(t)dt \right]^{2.5} \left(t_2 - t_1 \right) \qquad [1]$$

where t is the time in seconds and a(t) is the acceleration in units of g. A critical value of 1000 generally being the failure point in most standards, and a maximum elapsed time ($t_2 - t_1$) of 15 ms is often used (23, 29). However, Newman has presented results of other researchers and suggested HIC should be used cautiously because a proven correlation has not been developed between HIC and the severity of head injury (23).

Similarly, the SI function (Equation 2) was also developed from the Wayne State curve (8, 14, 15, 23) and also utilizes the acceleration (g) and time (seconds).

$$SI = \int_{t_1}^{t_2} a(t)^{2.5}\, dt \,. \qquad [2]$$

The SI is commonly used in National Operating Committee on Standards for Athletic Equipment (NOCSAE) testing standards (along with the maximum linear acceleration)

where a failure threshold of 1200 is used (19, 24, 26). This is often referred to as a weighted impulse-time criterion (8, 12). It should be noted that the 2.5 power used in both the HIC and SI equations comes from the slope of the Wayne State curve in a log-log plot (27).

In a 1980 paper, Newman stated that a "correlation of internal head injury with linear parameters only, presumes that either rotational effects are negligible or that they are somehow automatically accounted for in the measurement of linear acceleration" (23). With the two most common head injury assessment functions in use, SI and HIC, being dependent only upon the linear acceleration (14, 15, 24, 27), Newman suggested the use of the GAMBIT function (Equation 3) based upon the idea that "the onset of brain injury occurs when the combined effect of translational and rotational acceleration exceeds some limiting value" (21).

$$G(t) = \left[\left(\frac{a(t)}{250} \right)^2 + \left(\frac{\alpha(t)}{25000} \right)^2 \right]^{1/2} \qquad [3]$$

GAMBIT "endeavors to take into consideration the combined effects of both translational and rotational kinematics" (21). The values of 250 and 25000 seen in Equation 3 are critical values of the linear acceleration (g's) and rotational acceleration (rad/sec^2), respectively, that were developed for use in the determination of GAMBIT. Likewise, the values of a and α in Equation 3 are the linear and rotational accelerations with units of g and rad/sec2, respectively. It should be noted that since the acceleration terms are a function of time so is GAMBIT, even though only the peak value is generally of interest (21, 24).

Of the previously mentioned assessment functions for head injury, the most recently developed is the Head Impact Power (HIP). The HIP is based upon the rate of change of kinetic energy experienced by the head in each of its six degrees of freedom (15, 27) as seen from Equation 4.

$$HIP = 4.50a_x \int a_x dt + 4.50a_y \int a_y dt + 4.50a_z \int a_z dt + 0.016\alpha_x \int \alpha_x dt + 0.024\alpha_y \int \alpha_y dt + 0.022\alpha_z \int \alpha_z dt \qquad [4]$$

The coefficients presented in Equation 4 mass and mass moments of inertia of the human head as presented by Newman, et al (27). The HIP equation takes into account the issue of directional sensitivity of the brain (10, 27) since the response of the brain will have a "different tolerance to power absorption in each of the different directions and for each axis of rotation" (27). Based on the study by Newman, et al (27), it was concluded that the maximum value of HIP "appears to correlate better than existing head injury assessment functions." The curve for probability of concussion that was developed demonstrated a "gradual increase in the probability of MTBI with increasing HIP_m" where a value of 12.8 kW results in a 50% probability of concussion (27).

One thing to keep in mind when considering any head injury assessment function is that not every person will have the same tolerances, which can vary based on a number of factors such as age, head size, etc. (11, 18). The assessment functions have been developed by research involved with testing on animals, human cadavers, human volunteers (for non-injurious testing), and accident/impact reconstruction using human surrogates, most notably instrumented dummies and headforms (16, 18, 26). In recent years, there has been the development of computer and finite element models of the human head and brain to depict the general behavioral characteristics in specific situations, such as the Wayne State University Brain Injury Model, or WSUBIM (34).

2.2 Principles of Head Protection

Helmets are used in numerous sports, recreational activities, and occupations in which there is a risk of injury to the head. Their sole purpose is to protect the head. This is achieved by reducing the likelihood of an injury by lowering the severity of the impact being transferred to the head by means of energy attenuation. In simpler terms, a helmet serves to reduce the peak force of an impact on the head by increasing the time duration over which the impact occurs. This is similar to how an airbag in an automobile accident decreases the rate of deceleration of a passenger by allowing the deceleration event to take place over a longer period of time (12, 15, 22).

With it being virtually impossible to predict every possible scenario of head impact and design a helmet to protect in all of these cases (22), helmets are often designed to be used in particular situations, such as bicycling, skateboarding, football, baseball, hockey, motor sports, etc. By focusing on specific types of use, a helmet can be designed to achieve the best level of protection against impact scenarios that are likely to be encountered in that specific activity (14, 15, 22). The ultimate goal is to develop a helmet that can provide the highest probability of protecting the wearer from the likelihood of injury for its given purpose. Numerous standards have been developed by organizations (such as CPSC, ASTM, and NOCSAE) that helmets must meet to certify that a given style of helmet will provide an acceptable level of protection to the wearer, if used properly (1, 4, 14, 15, 19, 22, 25).

2.2.1 Helmet Design and Function

A helmet is generally comprised of at least two parts: the liner and the shell. Most helmets also consist of some form of softer materials inside the helmet to assist in the comfort and fit of the helmet, but do not serve any role in head protection. The shell is the outer part of the helmet, generally the hardest and toughest part of a helmet, and is usually made from some type of polymer or composite material. The liner is the part between the head and the outer shell that provides most of the attenuation of energy. The liner is most commonly comprised of some sort of padding or foam that will deform enough to "absorb" the energy of an impact. There are also some helmets that are practically shell-less or have a "micro-shell," such as most bicycle helmets (14, 15, 22).

The outer shell of a helmet serves to distribute the force of an impact over a larger area of the helmet, as well as providing a defense against penetration of an object through the helmet (15, 22). In general, a material chosen for a helmet shell should be strong with a high stiffness and strength-to-weight ratio. A smooth finish is "desirable as it will limit the generation of tangential forces" that will "generate a torque that in turn may produce angular acceleration" (22).

As stated earlier, the helmet liner serves as an energy attenuator. During an impact, the liner should deform, or crush, essentially acting as a cushion to reduce the force transmitted to the head. It is important that the material chosen will provide an adequate

crushing strength to ensure that it will deform at a fairly constant rate and at forces below the levels that would result in an injury to the head. The liner should be thick enough to deform to the highest expected forces that would be involved in its particular use so that the liner does not bottom out, or crush completely. If this were to occur, once the material has crushed to its maximum it would no longer absorb any of the energy and the remaining energy would be transferred directly to the head. The material should also have low rebound characteristics (hence, a plastic deformation, such as a single-use bicycle helmet) so there would not be a large change in the velocity of the head, which could result in a more severe injury to the brain than the force of the impact itself (12, 15, 22).

The helmet shell and liner work in conjunction to protect the head. The shell serves to spread the impact force over a larger area. The liner will then crush under the distributed load and attenuate as much energy as possible to reduce the force transferred to the head. Some helmets, such as bicycle helmets, are usually designed for single use where once they have sustained an impact, the materials are permanently deformed and, thus, will not recover to protect in a second impact. Others, such as football helmets, are designed for multiple impacts, so a liner material must be chosen that will recover from an impact after a period of time in order to protect the wearer for any subsequent impacts (14, 15, 22).

2.2.2 Organizations and Standards

A number or organizations are in place to protect the consumer by ensuring that helmets designed for a particular activity, such as football, will perform adequately to protect the wearer against expected impact conditions. Some of these organizations include the American Society for Testing and Materials (ASTM), the Consumer Product Safety Commission (CPSC), and the National Operating Committee on Standards for Athletic Equipment (NOCSAE). There are specific standards for specific types of helmets (such as bicycle, motorcycle, football, baseball, hockey, equestrian, and even military helmets) that contain precise testing methods and procedures, with certain criteria that must be met in order for the helmet to receive a passing rating (1, 4, 15, 19, 25).

Testing standards for helmets generally require multiple impact locations at specified impact velocities (impact energies), with some standards requiring multiple hits in the same location, on specified test anvils and impact surfaces. A common requirement in many

standards necessitates helmets be tested at various specified temperature ranges and environmental conditions to ensure satisfactory performance regardless of what climate or weather in which they may be used. The standards not only address the impact characteristics of the helmet, but also any part of the helmet that is vital to the wearer, such as facemasks or retention systems, must meet specific performance requirements. As addressed before, the linear impact condition is currently the only scenario examined in testing standards (1, 4, 14, 15, 19, 25).

2.3 Rotational Acceleration of the Head

Margulies, et al (16, 17, 18) performed studies with the effects of rotational-induced accelerations in the brains of primates, including the study of shear strains in the brain that are associated with DAI. In their research, they studied the kinematic effects on the head of primates through the use of animal testing, physical experiments, and analytical models. A goal was to attempt to develop a DAI tolerance criterion for a human that takes into account kinematics of the head and the mass of the brain, which is not accounted for in the HIC function. It was suggested that the best predictors to use as a threshold for DAI are the peak angular velocity and peak angular acceleration. Also, even through the center of rotation of a head in the normal range of motion does not occur at the CG of the head but in the neck, it was determined that "a non-centroidal rotation of the head can be approximated by a centroidal rotation of the same magnitude" (16).

The results of the models and animal tests were then used to determine a critical stain value associated with DAI in the baboon, which were then scaled to apply the tolerance for humans. A curve based on the peak change in rotational velocity and the peak rotational accelerations was developed that approximates the threshold where DAI would occur over a range of brain masses in humans. An onset of moderate-to-severe DAI was approximated as occurring at a rotational acceleration of 1.6×10^4 rad/sec^2 (18). The concussive threshold was concluded to be at much lower levels of rotational accelerations than those that would result in DAI (17).

Fijalkowski, et al conducted a study of severity of diffuse brain injury (DBI) in rodents based on linear-induced rotational acceleration. In their study they suggest that similar biomechanical correlations exist between the inertial loading of rats and humans. When looking at the resulting unconscious time in the rat based on a rotational input, it was determined that the HIP function provided significantly better correlations to the length of unconsciousness than GAMBIT or peak rotational acceleration. They concluded that "severity of head injury cannot be expected to vary linearly with amplitude alone" and that the duration of the rotational acceleration should also be taken into account, as the HIP function does (6, 7).

Research performed by Zhang, et al, at Wayne State University utilized a finite element model of the human head to analyze 24 head-to-head football impacts in an attempt to develop MTBI thresholds based upon shear stresses and intracranial pressures experienced in the brain. In their research, they determined that linear accelerations could be used as a good predictor of intracranial pressure in the brain, while rotational accelerations were not reliable predictors of the intracranial pressure. However, in the case of maximum shear stresses in the brain, there was strong sensitivity to rotational accelerations with no reliable correlation associated with linear acceleration (34).

Additionally, Zhang, et al, presented a range of parameters that would result in certain probabilities of concussion, and compared their results to injury thresholds proposed by the research of others. These included linear and rotational accelerations, along with HIC and shear stress at the brain stem. When analyzing the HIC, they noted that an 80% probability of concussion occurred at a value of 369, well below the 1000 failure limit used in standards (34). The tolerance limits developed by Zhang, et al, were virtually the same as those presented by Newman, et al (24), which also included additional tolerance limits for concussion based on SI, GAMBIT, and maximum HIP. These results are summed up in Table 2.1 and will be used as reference limits in this study.

Table 2.1 - MTBI thresholds developed by Zhang, et al (34) and Newman, et al (24)

Chance of MTBI	Linear * (g)	Rotational * (rad/sec^2)	HIC_{15}*	SI †	GAMBIT †	HIP_{max} † (kW)
25%	66	4600	151	185	0.33	9.8
50%	82	5900	240	290	0.39	12.8
80%	106	7900	369	415	0.47	16.5

* Results presented by Zhang, et al (34)
† Approximated from MTBI probability curves presented by Newman, et al (24).

2.4 NFL Study on MTBI

Due to the ongoing problem of concussion suffered by players in professional football, the National Football League created a committee in 1994 to study MTBIs that occurred in NFL games. The committee was composed of a diverse group that included the likes of physicians and trainers in the NFL, as well as experts in traumatic brain injuries. Between 1996 and 2001, the committee gathered information about MTBIs that occurred in the NFL along with game videos of the impacts to perform laboratory reconstructions of specific incidents (24, 25, 26, 28, 29, 31).

One hundred eighty-two cases were selected, eventually narrowed to 27 cases (22 of which involved diagnosed concussion) that provided only helmet-to-helmet hits. When including helmet-to-ground hits, there were 31 total cases, of which 25 involved concussions. All of the cases that were analyzed provided adequate video views to determine the velocity vectors at impact. The reconstructions, as discussed by Pellman, et al (28, 29, 31) and Newman, et al (24, 25, 26), involved the use of Hybrid III heads and necks, which are anthropometric test dummies often used in automotive testing. The Hybrid III heads were instrumented with accelerometers in a 3-2-2-2 configuration (three accelerometers at the center of gravity of the head to measure linear motion with coupled

pairs of accelerometers that capture the rotational motion about each axis) to measure rotational acceleration (26, 28).

In the reconstructed cases, when a concussion was involved, the struck player was always the one concussed while the striking player never received a concussion (29). It was determined that the striking player virtually always struck with the top of the helmet (which is the stiffest part of the helmet and generally the most resistant part of the head to concussions), while the struck player was most commonly stuck between the 90° quadrant between the front and side of the helmet. Nearly three-fourths of the players (from the reconstructed cases) struck in this region received concussion, and it was determined that the "maximum head acceleration occurred from an impact vector of 48.8° ± 18.0°" measured around from the front, where 0° is the front center of the head. Additionally, the higher risk of concussion of the struck player was likely influenced by the observation that there was an approximated 67% larger "effective mass of the striking player than that of the struck player during peak force" due to the fact that a striking player will often make impact with the head, neck, and torso all aligned, creating a larger amount of the body mass to be involved in the impact (29).

After analyzing the reconstructed data for all 27 helmet-to-helmet cases, it was determined that the average impact velocity was 9.3 ± 1.9 m/s. This resulted in peak linear values of the struck player's head being 76.9 ± 26.2 g's (94.3 ± 27.5 g's in 22 concussion-only cases) and peak rotational accelerations of 4289 ± 2156 rad/sec^2. It was concluded that rotational accelerations did not "identify a relevant correlation" in the NFL study and that the linear accelerations were the most important factor to study (31). However, based on the linear data of the reconstructed impacts, it was determined that the threshold for concussion in the NFL was approximately 7.4 m/s with an SI of about 250. The average velocity of 9.3 m/s had an SI of approximately 470 (30, 31).

- CHAPTER 3 -

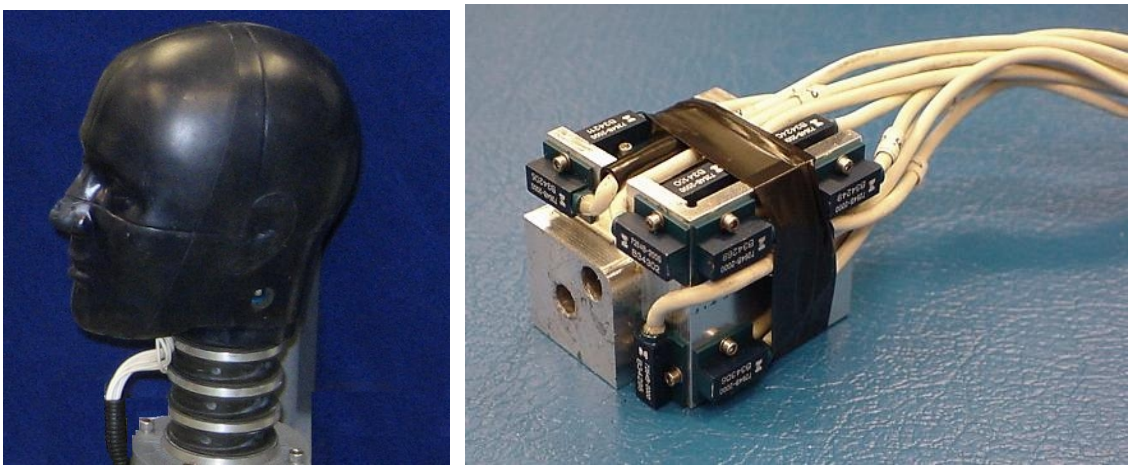
EXPERIMENT OBJECTIVE, SETUP, AND PROCEDURE

3.1 Objective of Experiment

The NFL study on MTBI concluded that rotational acceleration did not prove to be as important a factor to examine in concussion as linear acceleration (28, 29). This sparked some debate because it is counter to the belief that rotational acceleration is as important, if not more, than the linear acceleration effects (2, 9, 10, 15, 16, 18, 21, 22, 27, 28). In actuality, the most important determinant of injury may depend upon the impact situation.

This research aims to determine if, in different impact situations at the same energy levels, there is one form of acceleration that is consistently more significant than the other, or if it is all relative to the conditions of the specific impact situation. In order to evaluate this, it was decided to break the testing into multiple test conditions that would simulate different impact scenarios: some in which the head is in motion prior to impact, and others in which the head is stationary.

Bicycle helmets were used in the testing, which was beneficial due to the fact that they are single-use helmets with permanent mechanical deformations after impact. As a result, similar damage occurring at the same energy levels could easily be confirmed through visual inspection. Each helmet was impacted twice at the same energy level and test condition. The impact locations were the right and left sides, approximately 45° off the front of the helmet. This produced two data points for each helmet, assuming symmetric response of the helmet and headform. This impact site was chosen based on the results of the impact vector of 48.8 ± 18.0° from the NFL study, where the majority of their concussive events occurred in helmet-to-helmet impacts (29).



(a) **(b)**

Figure 3.1 - (a) Modified NOCSAE test headform with Hybrid III neck, and (b) 3-2-2-2 configuration of accelerometers on headform mounting block

3.2 Description of Equipment

The type of headform used in the testing was a modified NOCSAE medium headform that utilized a 3-2-2-2 accelerometer configuration attached to a Hybrid III neck. The NOCSAE headform is a biofidelic headform utilized in NOCSAE test standards (15, 19, 20). The Hybrid III neck is a segmented column made of rubber and aluminum that simulates the dynamic response of a human neck. The accelerometers used were Endevco Model 7246B-2000 shock accelerometers connected to an aluminum block in a 3-2-2-2 configuration, which was attached in the center of the head. The accelerometers were connected to an Endevco DC Differential Voltage Amplifier, which was attached to a National Instruments BNC-2090 connector box. The connector box sent the accelerometer data into the computer software via a NI-DAQ 6024E data acquisition card. The software used was BIODAQ 9-AX version 2.0b (Biokinetics and Associates Ltd., Ottawa, Ontario, Canada). The accelerometers were sampled at 10 kHz, with the outputs run through a 1000 Hz filter prior to being read by the software. The data was filtered additionally at 180 Hz in the software to remove any excess noise. See Figure 3.1 for views of the NOCSAE head,

Hybrid III neck, and accelerometer block. Additional information about the accelerometers and equipment can be found in the appendix. All testing was performed at Southern Impact Research Center (www.soimpact.com) in Rockford, Tennessee.

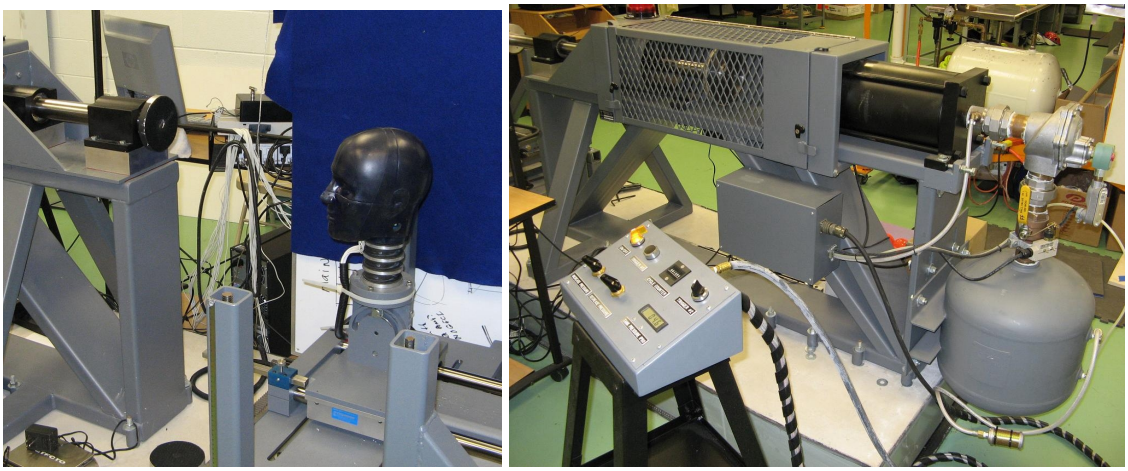
3.2.1 Drop Tower and Linear Impactor

The drop tower system, a common system in use in many testing standards (1, 4, 15), consisted of a NOCSAE head and Hybrid III neck attached to a carriage with linear ball bushings that freely moves along a monorail guide. The impact velocity is dependent upon the drop height of the carriage, which has a one-inch rigid protruding flag that moves through a velocity light gate during the free fall. The velocity gate will measure the speed just prior to impact and also serves as the triggering mechanism for the software to start receiving data from the accelerometers. Figure 3.2 shows a view of the drop tower system.



Figure 3.2 - View of Drop Tower System

The linear impactor is a relatively new experimental device that is being examined for use as a new testing system for the development and implementation of new testing standards being developed by NOCSAE (20). It was developed based on a similar pneumatic impactor developed at Wayne State University (30). The linear impactor system (see Figures 3.3 and 3.4) consists of a pneumatic ram that, once triggered, will release the buildup of pressure and propel an impact ram towards the headform that sits on a sliding sled base. The velocity of the impact is measured by means of a piston on the end of the ram moving through a velocity gate prior to moving into a tapered cylinder braking system that slows the piston down by compressing air trapped in the cylinder. The sled base the headform sits upon helps to absorb some of the energy after the initial impact. During a test, the measured impact scenario is completed well before any movement of the sled, as verified by the high-speed video, so the test headform receives the full energy of the impacting ram.



(a) **(b)**

Figure 3.3 - Linear impactor system with (a) view of head/neck assembly and end of ram, and (b) compressed air tank with control panel

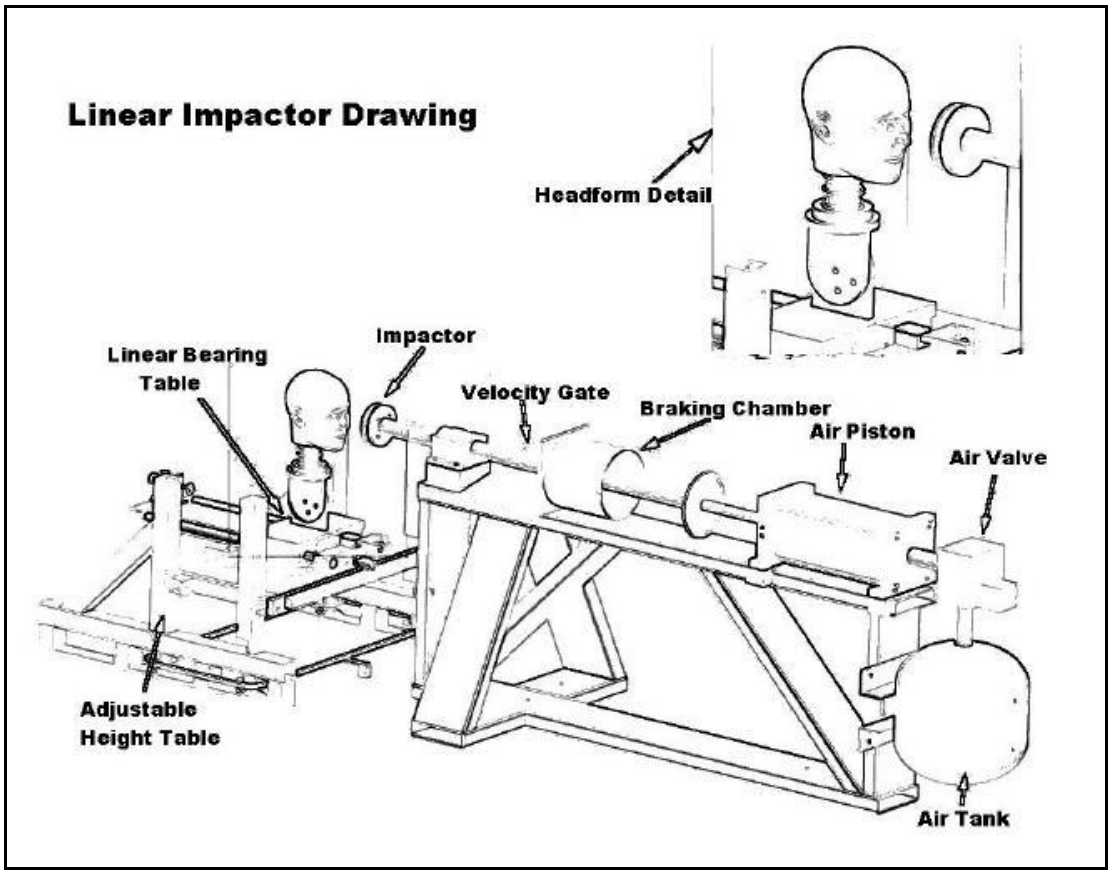


Figure 3.4 - Drawing of Linear Impactor System from NOCSAE (20)

The total drop mass of the head/neck assembly and carriage used in the drop tower system was 8.31 kg while the linear impactor ram has a mass of 14.37 kg. Due to the mass differences, the linear impactor would utilize lower impact velocities to match the same impact energy as the drop tower test conditions, based on the kinetic energy equation shown in Equation 5. The target velocities for the three energy levels used for each test condition can be seen in Table 3.1.

$$KE = \frac{1}{2}mv^2 \qquad [5]$$

Table 3.1 - Target velocities for specified energy levels used in test conditions

Target Energy (Joules)	Free Fall Velocity on Drop Tower (m/s)	Linear Impactor Ram Velocity (m/s)
77	4.3	3.3
121	5.4	4.1
160	6.2	4.7

3.3 Test Procedure

Four test conditions were selected: Conditions 1, 2, and 3 were tested on the drop tower system, while the linear impactor was used in Condition 4. Each test condition would be tested at three separate energy levels: 77, 121, and 160 Joules. Although much higher energy levels are obtainable on the linear impactor than on the drop tower, which is limited by the height of the system, the energy levels in this testing were limited to 160 J in order to prevent damage to the headform on the drop tower system tests. Larger impact energies were initially considered, but after several practice tests it was determine that repeated impacts at these energies would prove to be too violent to the headform.

Condition 1 was a vertical drop onto a flat anvil with a primary impact to the head where the neck was able to bend past the impact surface. It simulated an impact with the abrupt stop of one's head where the torso continued with its momentum after the impact. Conditions 2 and 3 were similar in that they were both vertical drops that simulated the torso/shoulder first impact where the head continued with its momentum and experienced an angular motion of the head created by the neck flexion. Condition 2 resulted in an impact of the head on the surface of a 45° anvil at the end of the angular motion of the head, while Condition 3 had the angular motion with no head impact. The final test, Condition 4, involved a moving mass impacting a stationary head. See Figure 3.5 through 3.8 for views of the test condition setups.



Figure 3.5 - View of test headform and flat anvil in Condition 1

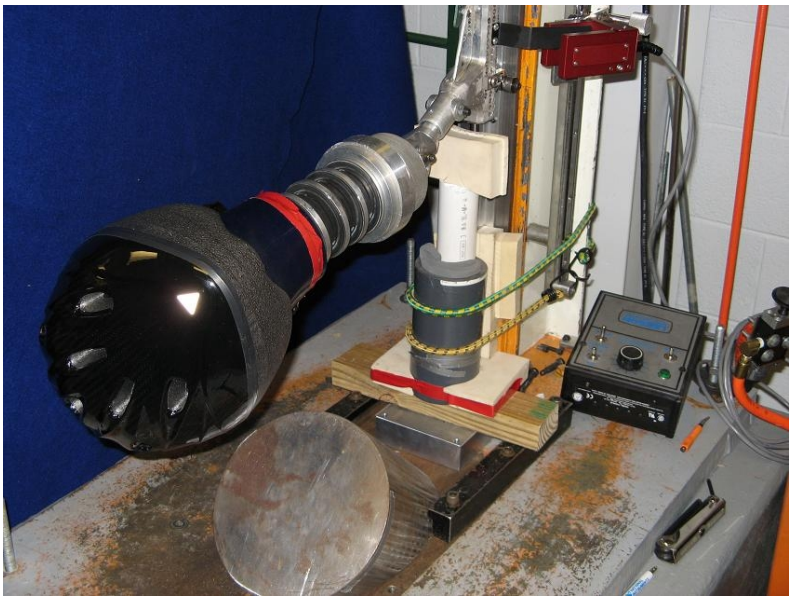


Figure 3.6 - View of setup for Condition 2

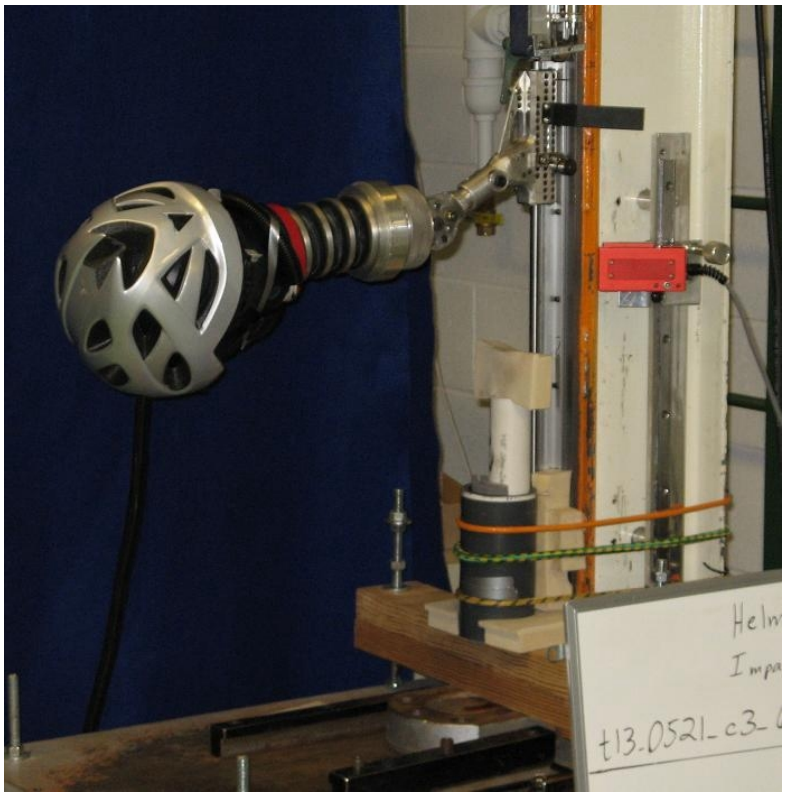


Figure 3.7 - View of test setup for Condition 3



Figure 3.8 - View of head and impactor ram in Condition 4

It should be noted that the abrupt stop to create the whipping motion of the head and neck used in Conditions 2 and 3 (see Figures 3.6 and 3.7) was done by a simple setup using a PVC pipe with a piece of high-density foam on the end to protect the test equipment. The carriage would freefall until hitting the stopping device and allowing the momentum of the head to continue. When viewing the high-speed video of the impact, the foam would crush to its maximum (about 2 inches) in approximately 10 ms, resulting in a negligible deceleration of the carriage.

Two types of helmets were used in the testing, which will be simply called X and Y to avoid using the manufacturer and/or model names. Helmet X was made of EPS (expanded polystyrene), which is probably the most common material used in bicycle helmets (15, 22), while the other helmet, Helmet Y, was constructed from EPU (expanded polyurethane). Both materials are lightweight and highly effective energy attenuators, but have very different manufacturing methods. As Newman (22) briefly describes, EPS can be produced quite easily to achieve consistent material properties. The EPU, however, can prove to be much more difficult to regularly obtain the same physical properties from batch to batch (22).

One of each type of helmet was used for each test condition and energy level, and, as stated before, each helmet was impacted twice, once on each side. The impact sites were labeled as A (right side) and B (left side). With four test conditions at three energy levels and two helmets with two impacts apiece, a total of 48 data points were obtained, 24 for each helmet. See Table A.1 in the appendix for a test matrix of the experiment results. Each helmet was impacted using the ASTM test line (1) based on a HPI of 25 mm. The test line, as seen in Figure 3.9, distinguishes the boundary for a legal hit in a testing standard, where the center of an impact must be at or above the test line.

The BIODAQ software recorded the linear accelerations of each of the nine accelerometers. The six accelerometers that are not capturing the linear acceleration at the head CG have their results processed through an algorithm that determines the rotational characteristics of the impact. The outputs include the time traces of the rotational and linear accelerations for each coordinate axis and the resultant values, and the overall peak values experienced. In addition, the software is able to calculate a number of head injury assessment functions including the HIC, SI, GAMBIT, and HIP.



Figure 3.9 – Arrow shows impact test line

All of the impacts were recorded using high-speed video at a rate of 1000 frames per second. Both the high-speed video camera and the BIODAQ software were synchronized to trigger off the velocity gates for the drop tower and linear impactor. With the high-speed video, it was possible to view exactly what is occurring during the approximately 100 ms impact, as well as to verify that the time traces of the accelerations logically correspond with what is physically happening to the helmet, head, and neck. See Appendix B for sample views of the high-speed video impacts at each energy level for the four test conditions.

- CHAPTER 4 -

RESULTS

Once the testing was completed, the data was analyzed by test condition and energy level, as can be seen in Figures 4.1 through 4.6. To aid in determining the concussion probability for each of the values, the limits presented in Table 2.1 have been added to the plots. Based on the linear acceleration (Figure 4.1), it can easily be seen that Condition 1 resulted in the largest values for a given energy level. Conditions 2, 3, and 4 were more similar in their linear values, even though they were different impact situations. It should be noted that Conditions 2 and 4 had an impact to the head while Condition 3 did not. Also, Conditions 2 and 3 were the same situational setup, only with an impact occurring in Condition 2, which, as expected, resulted in larger linear values.

When the rotational aspects are examined, there is a slightly different comparison between the different test conditions that could be seen in the linear case. Figure 4.2 shows Condition 4 definitely had the lowest values per energy level, while the rotational accelerations in Conditions 1, 2, and 3 were very comparable. This helps address a purpose of this study in understanding the relationship between the linear and rotational accelerations as being dependent upon the impact situation. Conditions 1, 2, and 3 all produced very similar rotational values for dissimilar linear accelerations, while Condition 4 had virtually the same linear accelerations as Condition 3, but the difference in their rotational accelerations were quite large.

Values of the head injury assessment functions SI, HIC, GAMBIT, and HIP can be seen in Figures 4.3, 4.4, 4.5, and 4.6, respectively. Naturally, the HIC and SI follow similar trends as the linear accelerations mentioned earlier. The GAMBIT and HIP, both of which are calculated from both the linear and rotational accelerations, each had the largest values per energy level in Condition 1 with the lowest in Condition 4. However, in Conditions 2 and 3 had very similar GAMBIT scores, but showed large differences in their maximum HIP values.

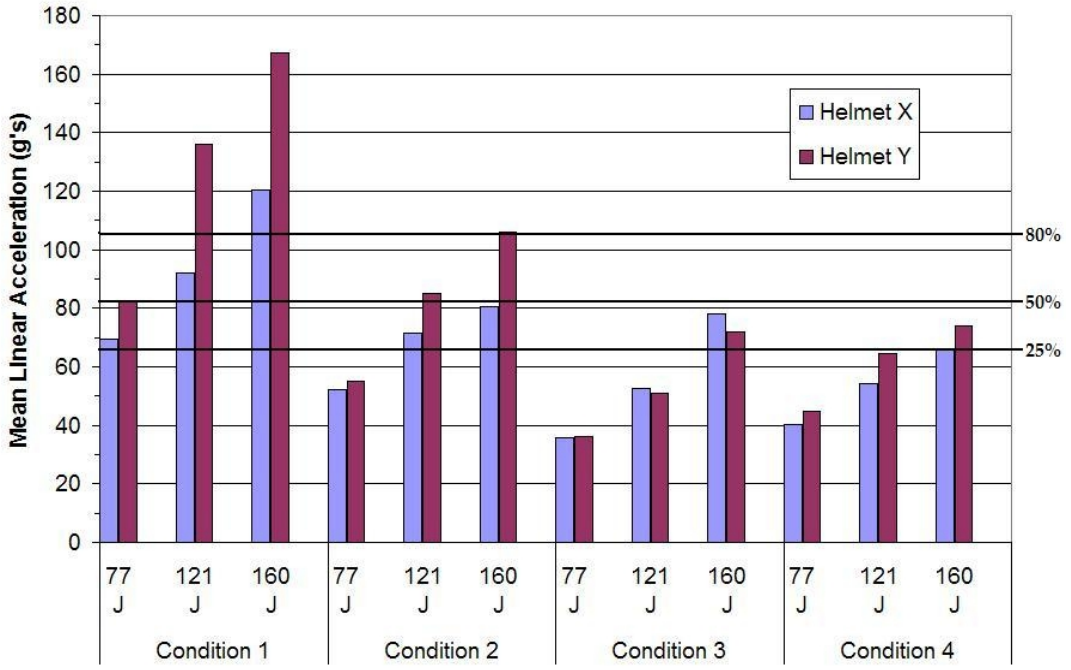


Figure 4.1 – Average of linear accelerations of locations A and B with concussion probability limits

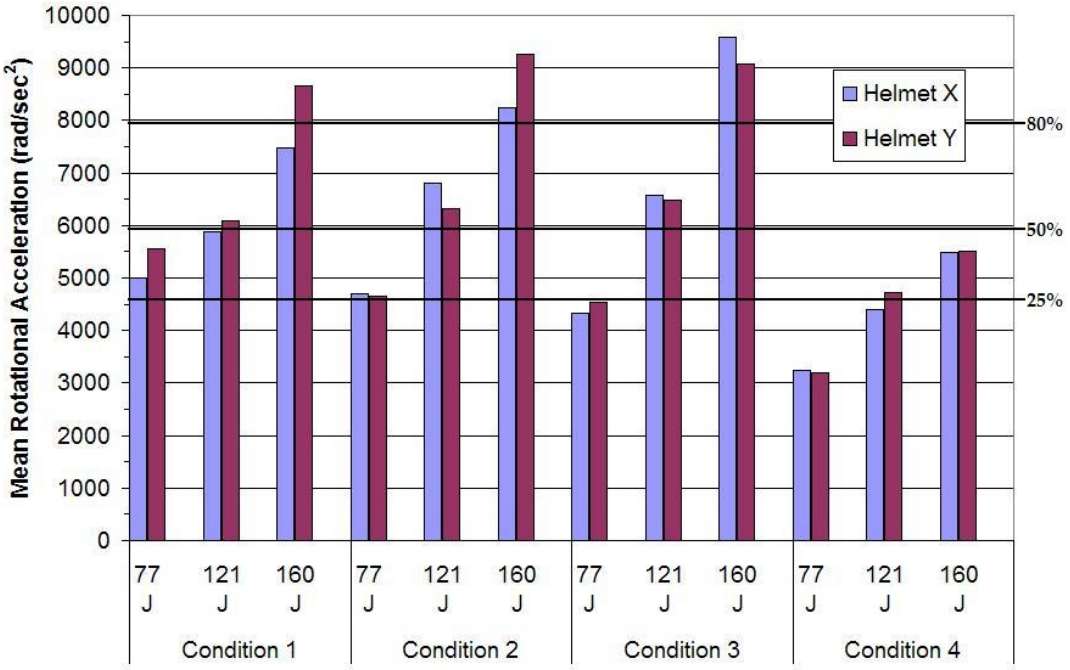


Figure 4.2 - Average rotational accelerations of locations A and B with concussion probability limits

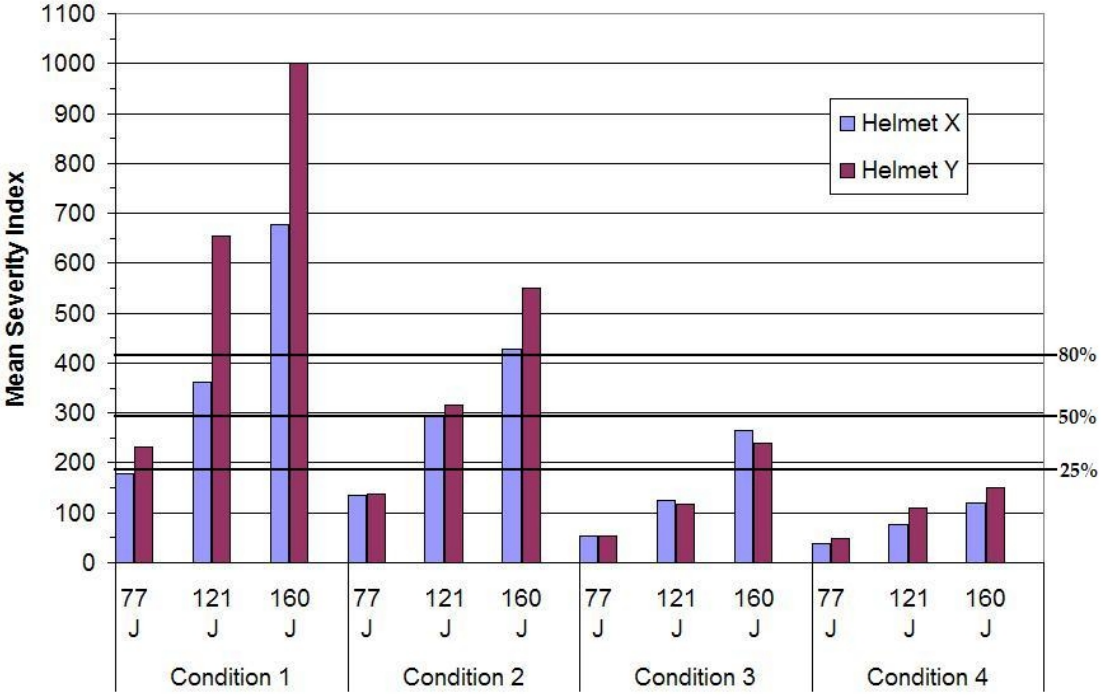


Figure 4.3 - Average SI of locations A and B with concussion probability limits

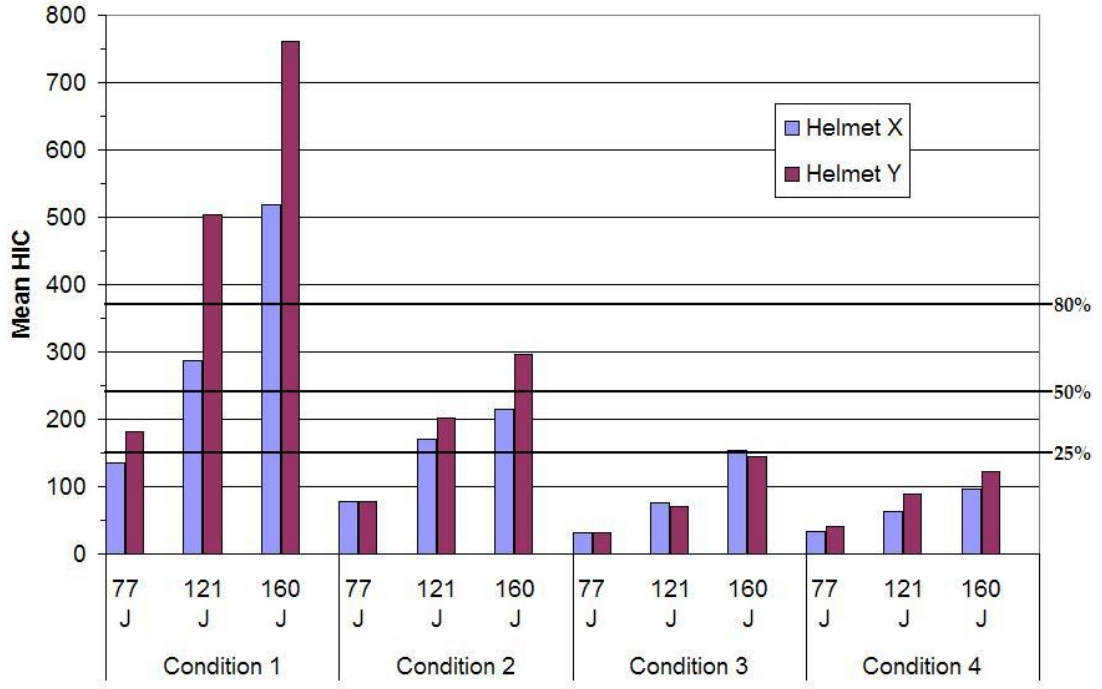


Figure 4.4 - Average HIC of locations A and B with concussion probability limits

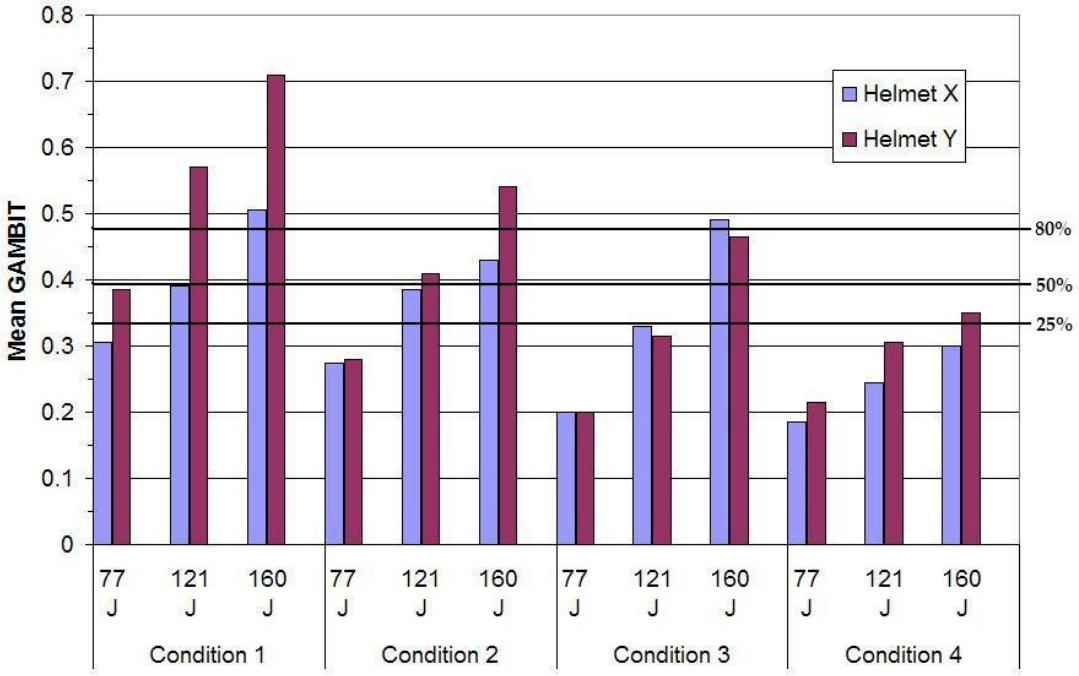


Figure 4.5 - Average GAMBIT of locations A and B with concussion probability limits

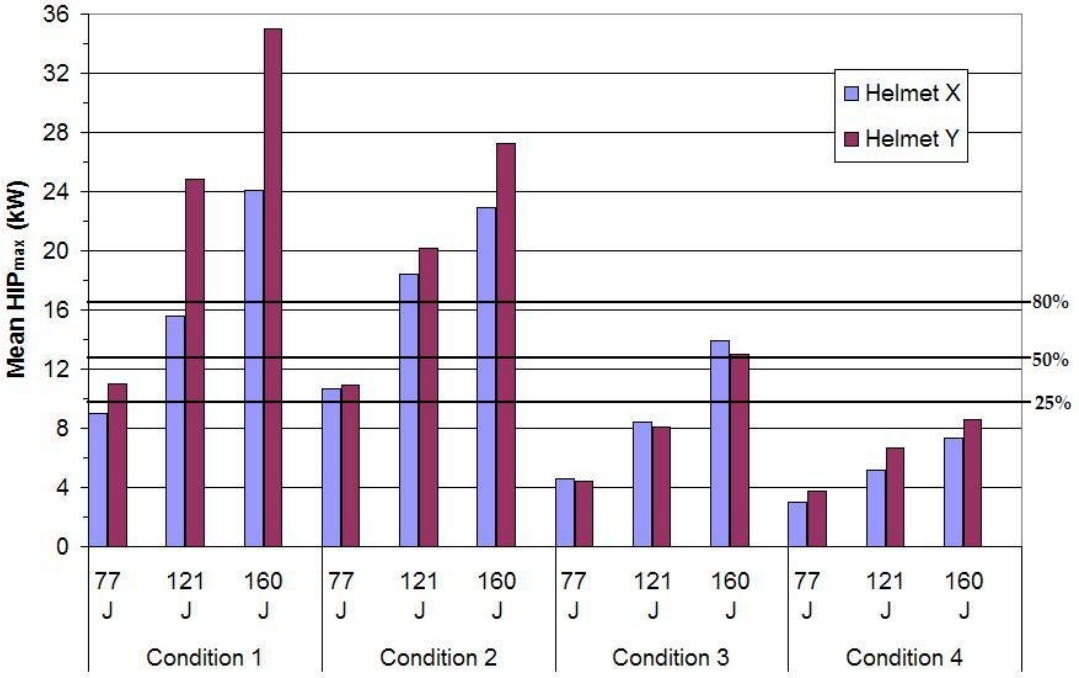


Figure 4.6 - Average maximum HIP of locations A and B with concussion probability limits

In general, when examining at the results between the two types of helmets, helmet Y tended to result in slightly higher values of the peak linear accelerations than helmet X, most notably in Condition 1, but there was not as drastic a difference when looking at the rotational accelerations. As a result of the linear values, the HIC, SI, GAMBIT, and HIP also tended to have their highest values with helmet Y in Condition 1.

Utilizing the results of the thresholds presented in Table 2.1, one could determine the probability of concussion for the results presented in this study. Based on the linear accelerations (see Figure 4.1), there would be less than a 50% chance of concussion in Conditions 3 and 4, but Condition 2 would possibly reach the 50% risk of concussion at the mid-level and higher impact energy levels. In Condition 1, the lowest energy level would have a 25-50% chance of concussion, while the higher energy levels would approach or surpass the 80% risk.

With the rotational values in Figure 4.2, virtually every scenario would result in at least a 25% risk of concussion, with the exception being the lowest energy level of Condition 4. The mid-level of energy in Conditions 1, 2, and 3 would result in a 50% concussion probability, while the 80% or greater chance could be expected at the highest energy level. Based on the HIP score (Figure 4.6), greater than an 80% chance of concussion could be expected in the higher energy levels of Conditions 1 and 2, while a 50% concussion risk could be expected in the highest energy level of Condition 3. The expected likelihood of MTBI based on the SI and HIC results in Figures 4.3 and 4.4, respectively, followed very closely to the expected probability based on the linear accelerations. This was to be expected, as they are a factor only of the linear terms. The GAMBIT (see Figure 4.5), which also takes the rotational values into account, showed a slight increase in the probability of concussion when compared with the linear injury assessment functions of SI and HIC under the same impact conditions.

To determine whether or not a correlation exists between the linear and rotational accelerations for the four test conditions, a linear regression of the data was performed in Microsoft Excel (Microsoft Corp., Redmond, Washington). As can be seen in Figure 4.7, the strongest correlation between the linear and rotational values exists in Conditions 3, $R = 0.990$ ($R^2 = 0.981$), and Condition 4, $R = 0.946$ ($R^2 = 0.895$). Condition 2, which was the same situation as Condition 3 but with an impact at the end of the whipping motion, had R

= 0.887 (R^2 = 0.787), while Condition 1 had the lowest level of correlation of all of the test conditions with R = 0.770 (R^2 = 0.593), and had the largest variance of data from the overall trend, as can be observed in Figure 4.7. The R-value is the correlation coefficient which represents measure of the linear association between the linear and rotational accelerations, where a value or R = 1.0 is a perfect linear fit. The R^2-values presented in Figure 4.7 are the coefficients of determination and report how the variance in the rotational acceleration is accounted for by the data fit, where the variance decreases as R^2 approaches 1.

When examining the performance of the individual helmets in each test condition (see Figures 4.8 through 4.11), it can be seen that helmet X and helmet Y provide similar linear trends between the rotational and linear accelerations in Condition 3 where there was no impact to the head. The trends of the two helmets in Condition 4 were slightly offset from one another, but each showed very strong linear correlations and similar slopes. Conditions 1 and 2 showed the most significant differences between the data trends of helmets X and Y, although Condition 2 showed much stronger linear correlations between the linear and rotational accelerations than Condition 1.

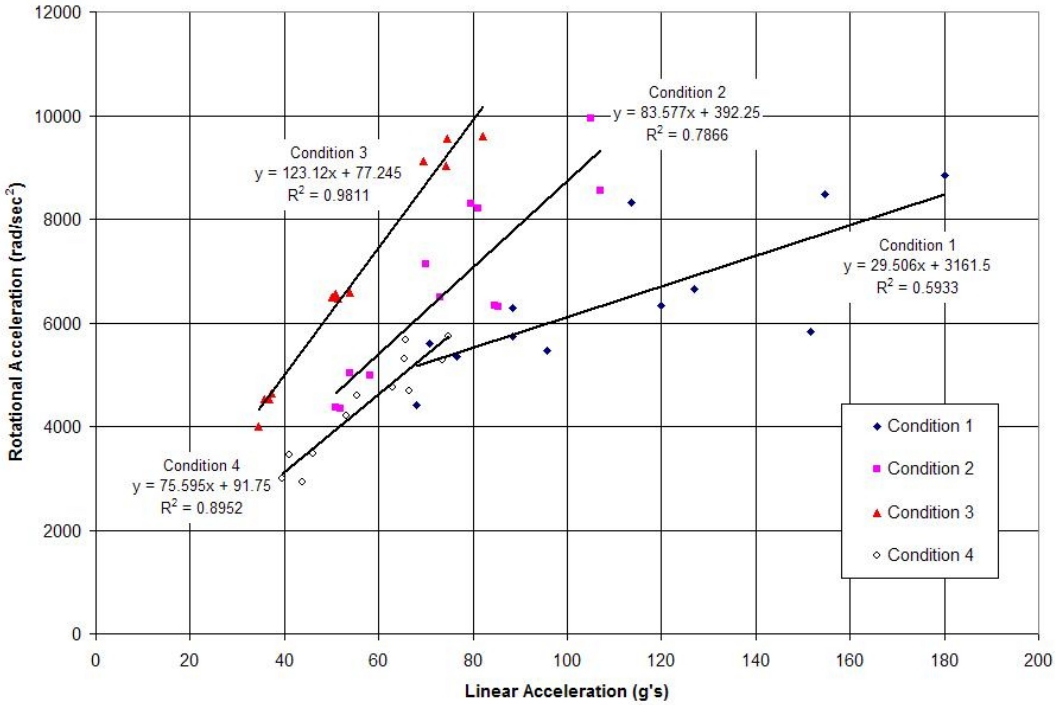


Figure 4.7 - Linear acceleration versus rotational acceleration per test condition

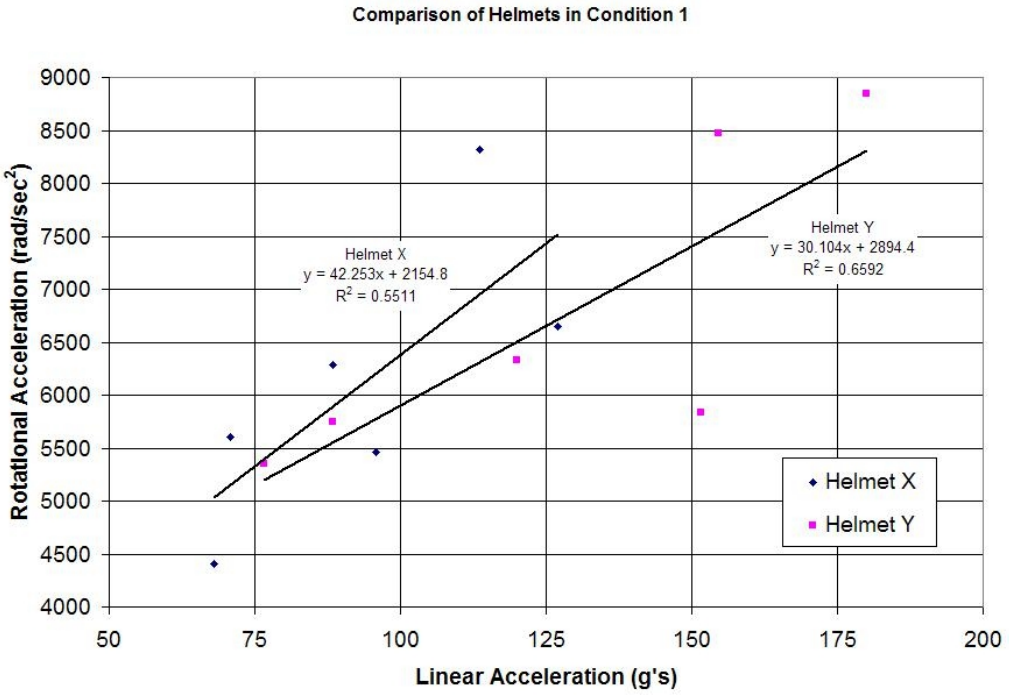


Figure 4.8 - Linear acceleration versus rotational acceleration in Condition 1

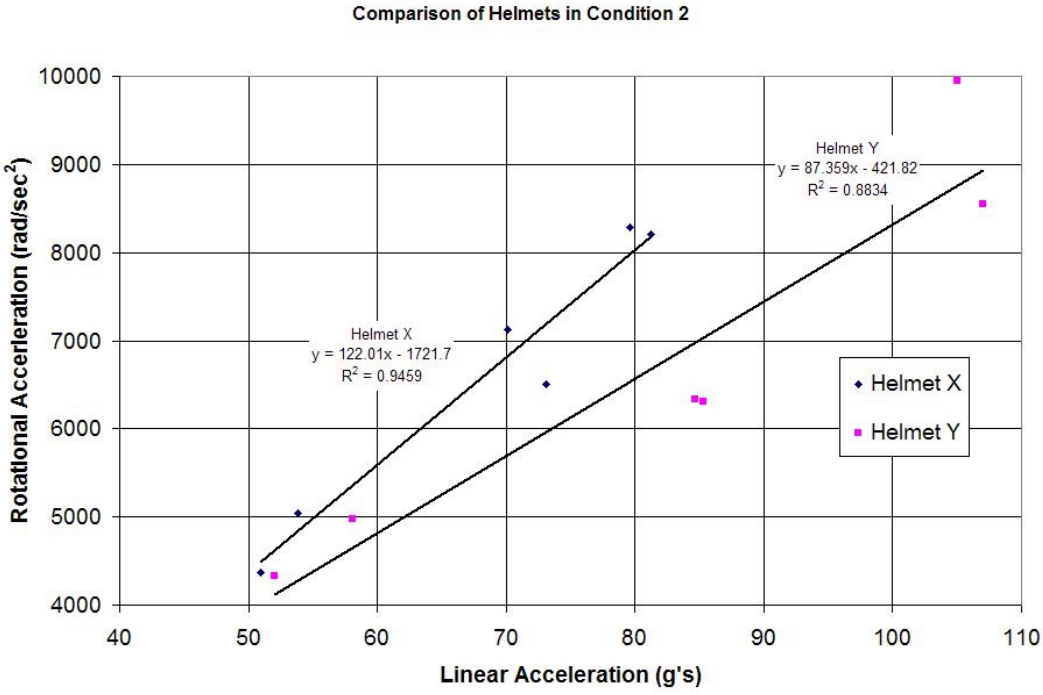


Figure 4.9 - Linear acceleration versus rotational acceleration in Condition 2

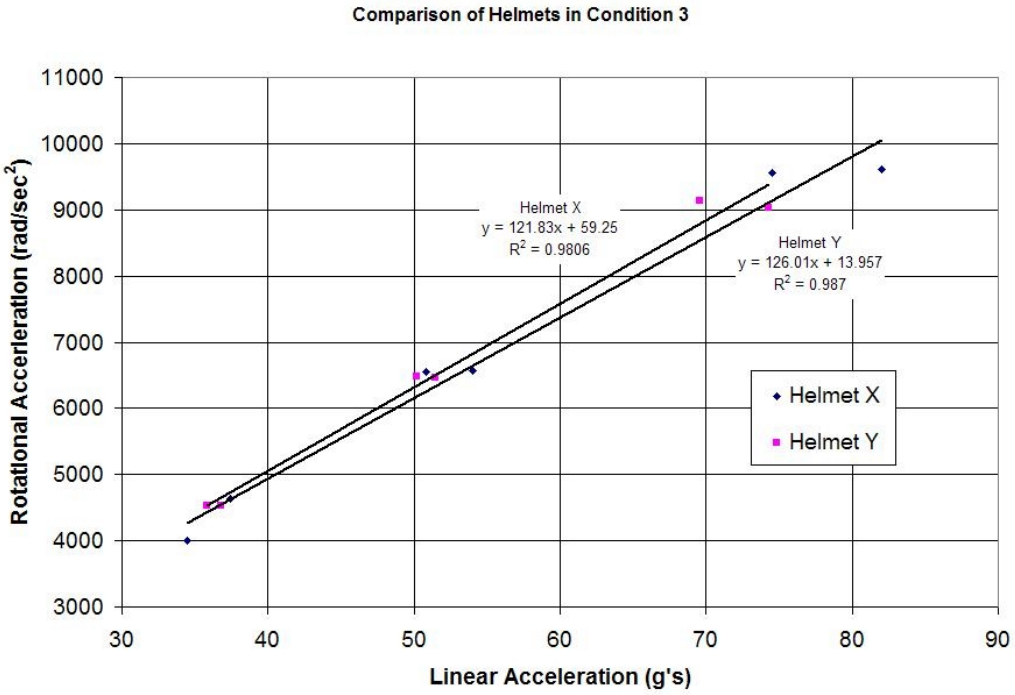


Figure 4.10 - Linear acceleration versus rotational acceleration in Condition 3

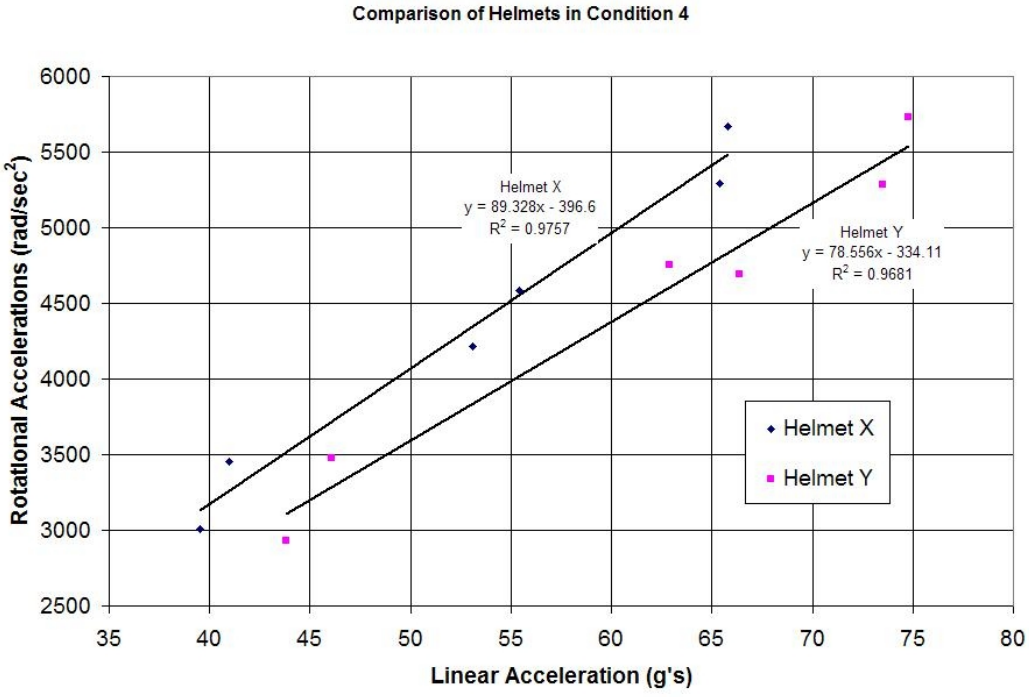


Figure 4.11 - Linear acceleration versus rotational acceleration in Condition 4

Due to the fact that there were two different types of helmets being tested in different test conditions and at different energy levels, it was desired to perform a statistical analysis to determine if there were significant differences in the results of the two styles of helmets. SPSS 15.0 (SPSS, Inc., Chicago, Illinois) was used to perform the statistical analyses in this study. A general linear model multivariate analysis was performed to observe the effects of the linear and rotational accelerations on the helmets through the various energy levels and test conditions. From this analysis, it was determined there was a much more significant effect contributed to the linear accelerations (p-value of 0.006) than the rotational (p-value of 0.511). This can be understood when examining Figures 4.1 and 4.2 where helmets X and Y produced very similar rotational accelerations in every scenario, but often had very different results in the linear acceleration terms.

A t-test was also performed, treating the two models of helmets as independent sets of data, to determine if there was a statistically significant difference between the results of the two helmet models. The results of the t-test can be seen in Table 4.1. The t-test was based upon a two-tailed distribution on a 95% confidence interval, so a p-value less than 0.025 would indicate a statistical significance. As can be seen by the values in Table 4.1, there was not a statistically significant difference between the two styles of helmets. The values of linear acceleration and GAMBIT produced more significant differences between the helmets than the HIC, SI, HIP, and rotational acceleration, which was the least significant. Additional statistics of comparing how the two helmet models performed against one another can be seen in Table 4.2.

Table 4.1 - t-test results at 95% confidence level

	t-value	df	p-value (2-tailed)
Linear (g's)	**-1.476**	**46**	**0.147**
Rotational (rad/sec^2)	**-0.358**	**46**	**0.722**
SI	**-1.016**	**46**	**0.315**
HIC	**-1.062**	**46**	**0.294**
GAMBIT	**-1.568**	**46**	**0.124**
HIP	**-1.022**	**46**	**0.312**

Table 4.2 – Standard deviations and true mean values of helmets X and Y

	Std. Dev. (S_X)		True Mean Value $\left(\bar{x} \pm \left(\frac{t \cdot S_X}{\sqrt{n}}\right)\right)$	
	X	**Y**	**X**	**Y**
Linear (g's)	**23.12**	**38.27**	**67.73 ± 6.97**	**81.20 ± 11.53**
Rotational (rad/sec^2)	**1835.4**	**1907.9**	**5976.8 ± 134.1**	**6170.1 ± 139.4**
SI	**184.56**	**289.48**	**229.13 ± 38.28**	**300.33 ± 60.03**
HIC	**134.99**	**217.18**	**154.71 ± 29.26**	**210.17 ± 47.08**
GAMBIT	**0.104**	**0.152**	**0.337 ± 0.033**	**0.395 ± 0.049**
HIP	**6.95**	**9.97**	**11.93 ± 1.45**	**14.46 ± 2.08**

Note: n = 24 each for helmets X and Y

- CHAPTER 5 -

CONCLUSIONS & RECOMMENDATIONS

From the results of this study, it can be concluded that the linear and rotational accelerations, in general, have a degree of linear correlation, but the variance and slope of the data trend varies considerably based upon the impact conditions. For a given value of linear acceleration at a specific impact energy, there can be a significant difference in the value of rotational acceleration for a head that is already in motion versus a head that is stationary. Additionally, for a head in motion, there can be significant differences in the linear acceleration for similar rotational values depending upon whether or not there is a direct or indirect impact to the head.

There was a stronger correlation between the linear and rotational accelerations in situations where the head is stationary and impacted by a moving object as opposed to when the head is in motion and strikes a stationary object. For the test conditions in which the head is the primary impact (Conditions 1 and 4) there was a drastic difference between the measured values linear and rotational accelerations of the head for the same initial levels of kinetic energy. If the head was in motion prior to impact, higher values of linear and rotational accelerations could be expected than when the head is stationary prior to being hit. This likely results from the fact that in Condition 1 the head is striking a stationary object that essentially has an infinite mass, while the impact scenario in Condition 4 involves the finite mass of the impacting ram striking the head.

The magnitude of the linear accelerations for a head in motion showed a strong dependence upon whether it was a direct impact of the head (as in Condition 1), or if the first impact was one that resulted in a whipping motion of the neck (Conditions 2 and 3) and a possible indirect impact of the head. The same could not be said of the rotational accelerations. For each case where the head was in motion prior to impact, high rotational accelerations were measured, all of which where larger than the rotational values when the head was stationary prior to the impact. In Conditions 2 and 3 where there is a whipping motion of the head, the peak rotational accelerations are approximately, the same regardless

of whether or not there is an impact to the head at the end of the motion, although an impact substantially increases the linear accelerations. Therefore, when the head does not experience the initial impact, (for example in a shoulder first impact scenario) it is possible to develop low linear, high rotational accelerations of the head.

Since helmets are designed to protect against linear impacts, different neurological outcomes at equal linear decelerations are likely to be associated with large differences in rotational acceleration. This is, of course, dependent upon the mechanisms involved in the impact. Based on these observations and the concussive tolerances developed by Zhang, et al (34) and Newman, et al (24), rotational acceleration should not be disregarded in a focus solely on the linear responses in head protection. Although the linear parameters may be adequate predictors of concussion in some situations, there is the possibility of scenarios in which the higher probability of MTBI will likely result more from the rotational accelerations than from the linear accelerations.

Therefore, both linear and rotational accelerations should be taken into account with the development of future helmet standards and injury assessment functions. This would require additional research on different types of helmets, as well as continued research into the human tolerance limits and injury assessment functions that are used as performance criteria in head protection standards. Since this research only involved bicycle helmets, it is recommended that the study be expanded to include different types of helmets (such as motorcycle, football, etc.), and possibly a larger sample of the number of helmets, in order to observe the mechanisms of impact through a larger data set.

REFERENCES

1. American Society for Testing and Materials (ASTM) F1446-02. "Standard Specification for Equipment and Procedures Used in Evaluating the Performance Characteristics of Protective Headgear." 2002.

2. Cantu, Robert C. "Biomechanics of Head Injury." Neurologic Athletic Head and Spine Injuries. Ed. Robert C. Cantu. Philadelphia: W.B. Saunders Company, 2000. 2-5.

3. Cantu, Robert C. "Overview of Concussion." Neurologic Athletic Head and Spine Injuries. Ed. Robert C. Cantu. Philadelphia: W.B. Saunders Company, 2000. 76-79.

4. Consumer Product Safety Commission (CPSC) 16 CFR Part 1203. "Safety Standard for Bicycle Helmets." March 1998.

5. Davis, C. H. "Self-Perception in Mild Traumatic Brain Injury." American Journal of Physical Medicine & Rehabilitation. 2002 Aug; 81(8): 609-618.

6. Fijalkowski, Ronald J., Ellingson, Benjamin, Stemper, Brian D., Yoganandan, Narayan, Gennarelli, Thomas A., Pintar, Frank A. "Interface Parameters of Impact-Induced Mild Traumatic Brain Injury." Proceedings of Rocky Mountain Bioengineering Symposium & International ISA Biomedical Sciences Instrumentation Symposium. 2006.

7. Fijalkowski, Ronald J., Stemper, Brian D., Pintar, Frank A., Yoganandan, Narayan, Gennarelli, Thomas A. "Biomechanical Correlates of Mild Diffuse Brain Injury in the Rat." Proceedings of Rocky Mountain Bioengineering Symposium & International ISA Biomedical Sciences Instrumentation Symposium. 2007.

8. Gadd, C.W. "Use of Weight-Impulse Criterion for Establishing Injury Hazard." Proceedings of Tenth Stapp Car Crash Conference. 1966.

9. Gennarelli, Thomas A. "Cerebral Concussion and Diffuse Brain Injuries." Head Injury. 2nd Edition. Ed. Paul R. Cooper. Baltimore: Williams & Wilkins, 1987. 108-124.

10. Gennarelli, Thomas A. and Thibault, Lawrence E. "Biomechanics of Head Injury." Neurosurgery. Ed. Robert H Wilkins and Setti S. Rengachary. New York: McGraw-Hill, 1985. 1531-1536.

11. Giza, Christopher C. and Hovda, David A. "Ionic and Metabolic Consequences of Concussion." Neurologic Athletic Head and Spine Injuries. Ed. Robert C. Cantu. Philadelphia: W.B. Saunders Company, 2000. 80-100.

12. Halstead, P. David. Private Communications (2007).

13. Hodgson, Voigt R. "Impact, Skid, and Retention Tests on a Representative Group of Bicycle Helmets to Determine Their Head-Neck Protective Characteristics." Report Prepared in cooperation with the Michigan Bicycle Helmet Advisory Committee and the Michigan Department of Public Health. Feb. 1990.

14. Hoshizaki, Thomas Blaine. "Engineering in Head Protection." Neurologic Athletic Head and Spine Injuries. Ed. Robert C. Cantu. Philadelphia: W.B. Saunders Company, 2000. 41-49.

15. Hoshizaki, T. Blaine and Brien, Susan E. "The Science and Design of Head Protection." Neurosurgery. 2004 Oct; 55(4): 956-967.

16. Margulies, Susan S., and Thibault, Lawrence E. "An Analytical Model of Traumatic Diffuse Brain Injury." Journal of Biomechanical Engineering. 1989 Aug; 111: 241-249.

17. Margulies, Susan S., Thibault, Lawrence E., and Gennarelli, Thomas A. "Physical Model Simulations of Brain Injury in the Primate." Journal of Biomechanics. 1990; 23(8): 823-836.

18. Margulies, Susan S., and Thibault, Lawrence E. "A Proposed Tolerance Criterion for Diffuse Axonal Injury in Man." Journal of Biomechanics. 1992; 25(8): 917-923.

19. National Operating Committee on Standards for Athletic Equipment (NOCSAE), doc. 001-06m07. "Standard Drop Test Method and Equipment Used in Evaluating the Performance Characteristics of Protective Headgear." January 2007. (http://www.nocsae.org)

20. National Operating Committee on Standards for Athletic Equipment (NOCSAE), doc. 081-04m04. "Standard Linear Impactor Test Method and Equipment Used in Evaluating the Performance Characteristics of Protective Headgear and Face Guards." January 2006. (http://www.nocsae.org)

21. Newman, James A. "A Generalized Acceleration Model For Brain Injury Threshold (GAMBIT)." Proceedings of International Conference of Biomechanics of Impact (IRCOBI). 1986.

22. Newman, James A. "Biomechanics of Human Trauma: Head Protection." Accidental Injury: Biomechanics and Prevention. New York: Springer, 1993. 292-310.

23. Newman, James A. "Head Injury Criteria in Automotive Crash Testing." Proceedings of 24th Stapp Car Crash Conference. 1980.

24. Newman, J., Barr, C., Beusenberg, M., Fournier, E., Shewchenko, N., Welbourne, E., Withnall, C. "A New Biomechanical Assessment of Mild Traumatic Brain Injury:

Part 2 – Results and Conclusions." Proceedings of International Conference on the Biomechanics of Impact (IRCOBI). 1999.

25. Newman, J., Beusenberg, M., Fournier, E., Shewchenko, N., Withnall, C., King, A., Yang, K., Zhang, L., McElhaney, J., Thibault, L., McGinnis, G. "A New Biomechanical Assessment of Mild Traumatic Brain Injury: Part 1 – Methodology." Proceedings of International Conference on the Biomechanics of Impact (IRCOBI). 1999.

26. Newman, J.A., Beusenberg, M.C., Shewchenko, N., Withnall, C., Fournier, E. "Verification of Biomechanical Methods Employed in a Comprehensive Study of Mild Traumatic Brain Injury and the Effectiveness of American Football Helmets." Journal of Biomechanics. 2005; 38: 1469-1481.

27. Newman, James A., Shewchenko, Nicholas, and Welbourne, Eric. "A Proposed New Biomechanical Head Injury Assessment Function – The Maximum Power Index." Proceedings of 44th Stapp Car Crash Conference. 2000.

28. Pellman, Elliot J., Viano, David C., Tucker, Andrew M., Casson, Ira R., Waeckerle, Joe F. "Concussion in Professional Football: Reconstruction of Game Impacts and Injuries." Neurosugery. 2003 Oct; 53(4): 799-814.

29. Pellman, Elliot J., Viano, David C., Tucker, Andrew M., Casson, Ira R. "Concussion in Professional Football: Location and Direction of Helmet Impacts – Part 2." Neurosurgery. 2003 Dec; 53(6): 1328-1341.

30. Pellman, E.J., Viano, D.C., Withnall, C., Shewchenko, N., Bir, C.A., Halstead, P.D. "Concussion in Professional Football: Helmet Testing to Assess Impact Performance – Part 11." Neurosurgery. 2006 Jan; 58(1): 78-96.

31. Viano, David C. and Pellman, Elliot J. "Concussion in Professional Football: Biomechanics of the Striking Player – Part 8." Neurosurgery. 2005 Feb; 56(2): 266-280.

32. Viano, David C., Pellman, Elliot J., Withnall, Chris, Shewchenko, Nick. "Concussion in Professional Football: Performance of Newer Helmets in Reconstructed Game Impacts – Part 13." Neurosurgery. 2006 Sep; 59(3): 591-606.

33. Warren, W. Lee, Bailes, Julian E., Cantu, Robert C. "Guidelines for Safe Return to Play After Athletic Head and Neck Injuries." Neurologic Athletic Head and Spine Injuries. Ed. Robert C. Cantu. Philadelphia: W.B. Saunders Company, 2000. 66-73.

34. Zhang, Liying, Yang, King H., and King, Albert I. "A Proposed Injury Threshold for Mild Traumatic Brain Injury." Journal of Biomechanical Engineering. 2004 Apr; 126: 226-236.

APPENDIX A

RAW DATA

Table A.1 - Raw data sorted by target energy level

Target Energy: 77 Joules

Test Condition	Helmet Style	Sample Number	Helmet Mass (grams)	Impact Location	Impact Number	Impact Velocity (m/s)	Impact Energy (J)	Linear Acceleration (g)	Severity Index (GADD)	Rotational Acceleration (rads/s^2)	HIC	GAMBIT	HIP (kW)
1	X	9	218.2	A	31	4.2905	76.49	70.8	184	5604.4	139	0.32	9.400
1	X	9	218.2	B	30	4.1639	72.04	68.1	171	4411.7	133	0.29	8.616
1	Y	13	343.5	A	35	4.3271	77.80	76.5	218	5346.3	172	0.36	10.419
1	Y	13	343.5	B	34	4.3271	77.80	88.3	244	5744.9	191	0.41	11.499
2	X	8	213.9	A	19	4.3051	77.01	53.8	136	5038.1	82	0.29	10.853
2	X	8	213.9	B	18	4.3419	78.33	50.9	133	4373.9	72	0.26	10.502
2	Y	12	349.5	A	20	4.3124	77.27	58.1	145	4980.0	85	0.30	11.606
2	Y	12	349.5	B	21	4.3271	77.80	52.0	130	4333.8	70	0.26	10.197
3	X	3	218.0	A	23	4.2905	76.49	37.4	56	4643.0	32	0.21	4.429
3	X	3	218.0	B	22	4.2689	75.72	34.5	51	4005.3	30	0.19	4.762
3	Y	6	333.7	A	24	4.2905	76.49	35.8	53	4522.9	30	0.20	4.293
3	Y	6	333.7	B	25	4.2833	76.23	36.8	52	4535.3	32	0.20	4.566
4	X	3	218.0	A	38	3.2439	75.61	41.0	39	3456.9	33	0.19	3.027
4	X	3	218.0	B	44	3.1950	73.34	39.5	37	3005.2	32	0.18	2.905
4	Y	6	333.7	A	41	3.1790	72.61	46.1	49	3479.3	42	0.22	3.984
4	Y	6	333.7	B	47	3.1377	70.74	43.8	46	2931.4	39	0.21	3.460

Target Energy: 121 Joules

Test Condition	Helmet Style	Sample Number	Helmet Mass (grams)	Impact Location	Impact Number	Impact Velocity (m/s)	Impact Energy (J)	Linear Acceleration (g)	Severity Index (GADD)	Rotational Acceleration (rads/s^2)	HIC	GAMBIT	HIP (kW)
1	X	1	219.3	A	5	5.3474	118.81	88.3	315	6285.7	252	0.39	14.632
1	X	1	219.3	B	6	5.3474	118.81	95.7	407	5457.2	322	0.39	16.556
1	Y	4	335.4	A	8	5.3474	118.81	151.7	773	5837.5	593	0.63	28.772
1	Y	4	335.4	B	7	5.3586	119.31	120.0	538	6328.8	416	0.51	20.882
2	X	2	215.8	A	1	5.3586	119.31	70.1	283	7125.1	166	0.39	18.195
2	X	2	215.8	B	2	5.3814	120.33	73.1	305	6501.8	175	0.38	18.689
2	Y	5	338.6	A	9	5.3586	119.31	85.3	307	6310.4	205	0.42	20.921
2	Y	5	338.6	B	10	5.3814	120.33	84.7	322	6329.6	198	0.40	19.361
3	X	3	218.0	A	4	5.3700	119.82	50.8	121	6553.9	72	0.32	7.713
3	X	3	218.0	B	3	5.3814	120.33	54.0	131	6575.3	81	0.34	9.074
3	Y	6	333.7	A	12	5.3474	118.81	50.2	114	6486.3	70	0.32	7.790
3	Y	6	333.7	B	11	5.3700	119.82	51.5	118	6471.6	72	0.31	8.313
4	X	15	218.3	A	39	4.1571	124.17	55.4	79	4585.7	66	0.26	5.406
4	X	15	218.3	B	45	4.0869	120.01	53.1	74	4213.2	61	0.23	4.983
4	Y	17	345.5	A	42	4.1605	124.37	62.9	102	4750.5	83	0.30	6.708
4	Y	17	345.5	B	48	4.1001	120.79	66.4	116	4694.0	96	0.31	6.580

Target Energy: 160 Joules

Test Condition	Helmet Style	Sample Number	Helmet Mass (grams)	Impact Location	Impact Number	Impact Velocity (m/s)	Impact Energy (J)	Linear Acceleration (g)	Severity Index (GADD)	Rotational Acceleration (rads/s^2)	HIC	GAMBIT	HIP (kW)
1	X	10	218.5	A	32	6.1650	157.92	113.5	642	8324.1	500	0.49	22.830
1	X	10	218.5	B	33	6.1800	158.69	127.0	711	6651.6	536	0.52	25.376
1	Y	14	340.7	A	36	6.1501	157.16	180.0	1133	8845.1	871	0.76	39.418
1	Y	14	340.7	B	37	6.2255	161.03	154.6	868	8476.9	650	0.66	30.593
2	X	7	220.4	A	14	6.1800	158.69	81.2	420	8209.0	207	0.42	22.545
2	X	7	220.4	B	13	6.2103	160.25	79.6	438	8286.3	222	0.44	23.217
2	Y	11	331.3	A	15	6.2103	160.25	105.0	533	9949.7	291	0.56	27.425
2	Y	11	331.3	B	16	6.2408	161.83	107.0	565	8555.1	302	0.52	27.123
3	X	3	218.0	A	28	6.1951	159.47	74.5	261	9565.6	155	0.48	12.831
3	X	3	218.0	B	29	6.2255	161.03	82.0	268	9606.7	154	0.50	14.993
3	Y	6	333.7	A	27	6.2255	161.03	69.6	245	9128.4	149	0.46	12.302
3	Y	6	333.7	B	26	6.2255	161.03	74.3	236	9035.4	141	0.47	13.640
4	X	16	217.5	A	40	4.7521	162.25	65.8	118	5667.5	95	0.31	7.668
4	X	16	217.5	B	46	4.7655	163.17	65.4	119	5294.7	96	0.29	7.024
4	Y	18	341.4	A	43	4.7700	163.48	74.8	149	5727.1	121	0.36	8.697
4	Y	18	314.4	B	49	4.6950	158.38	73.5	152	5282.4	125	0.34	8.507

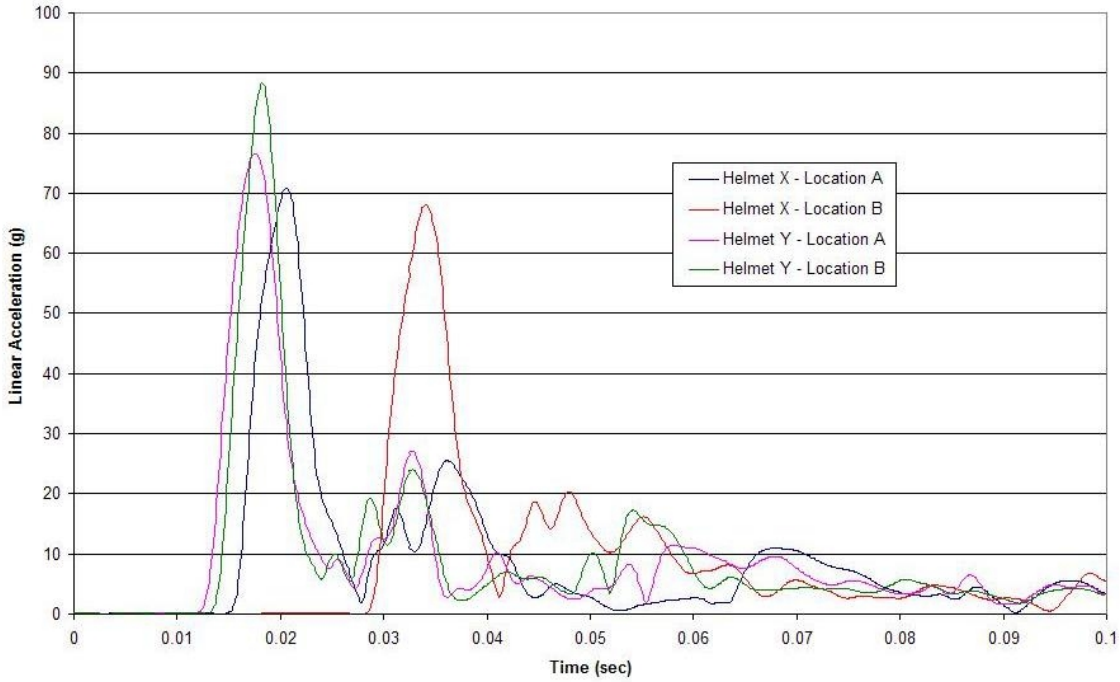


Figure A.1 - Linear acceleration time trace for Condition 1 at 77 Joules

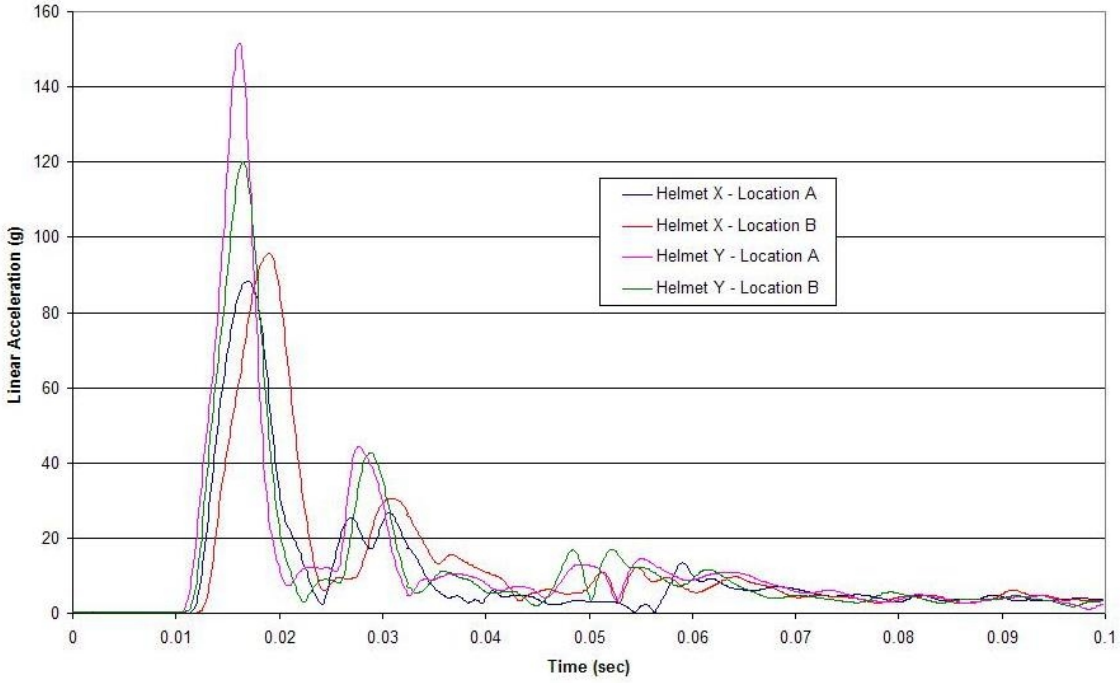


Figure A.2 - Linear acceleration time trace for Condition 1 at 121 Joules

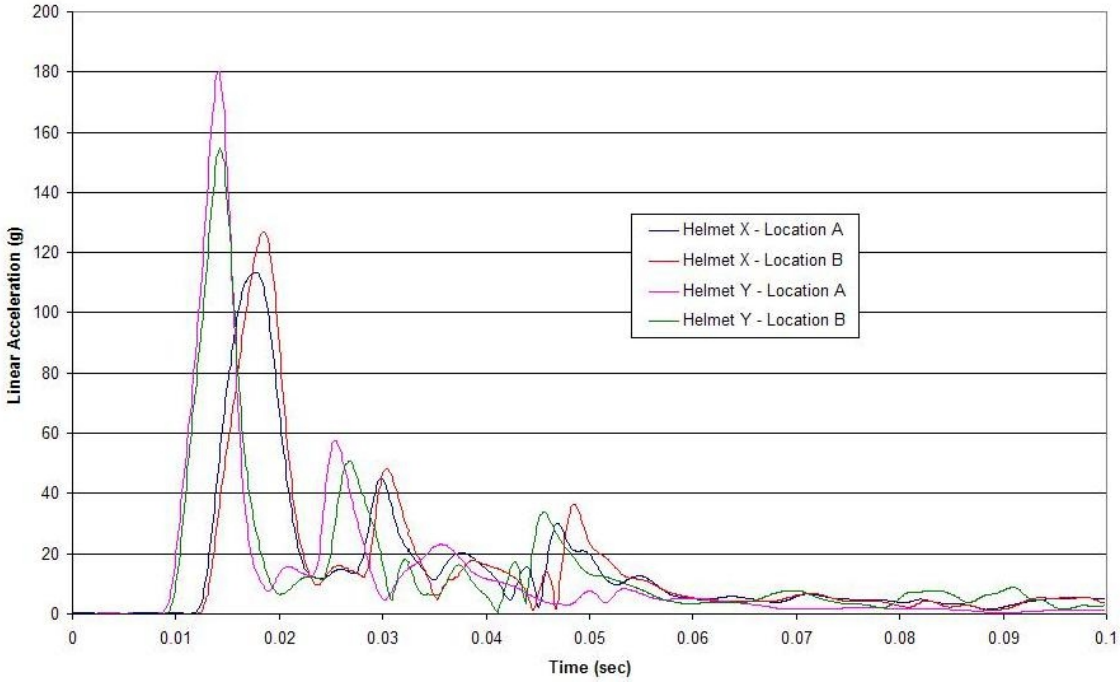


Figure A.3 - Linear acceleration time trace for Condition 1 at 160 Joules

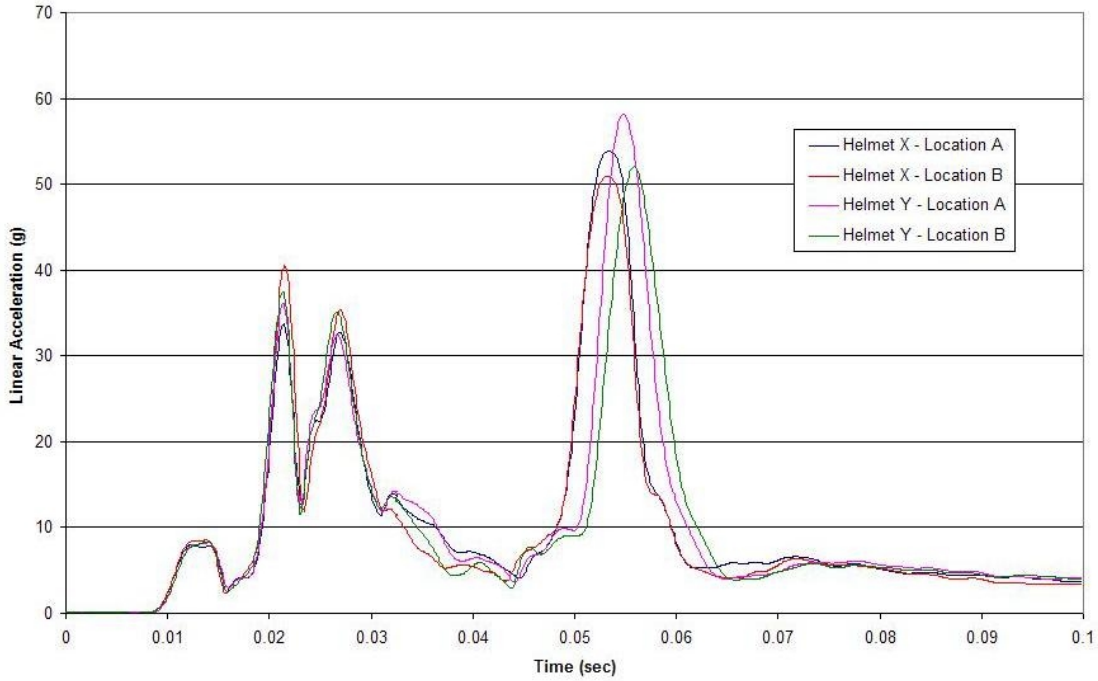


Figure A.4 - Linear acceleration time trace for Condition 2 at 77 Joules

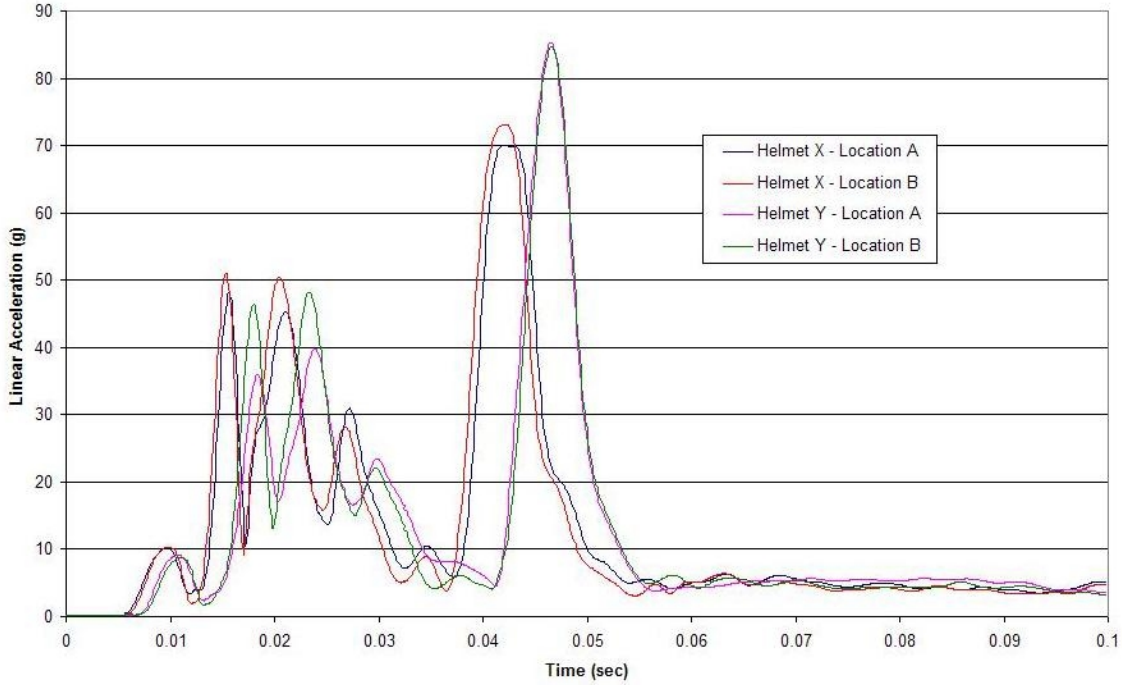


Figure A.5 - Linear acceleration time trace for Condition 2 at 121 Joules

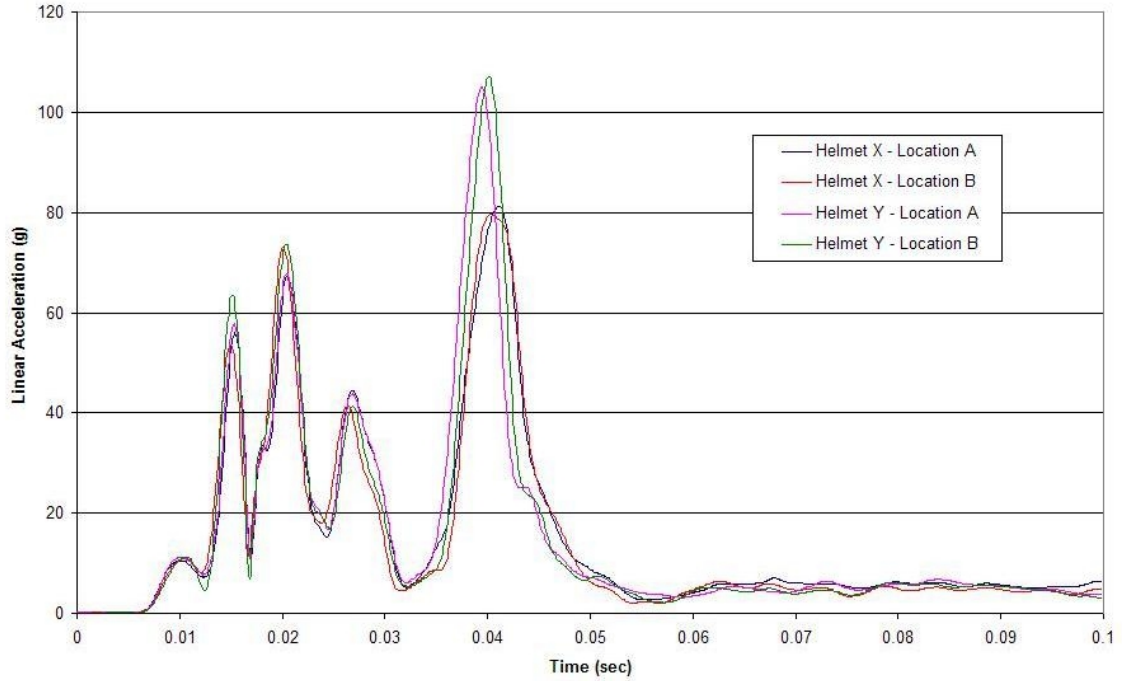


Figure A.6 - Linear acceleration time trace for Condition 2 at 160 Joules

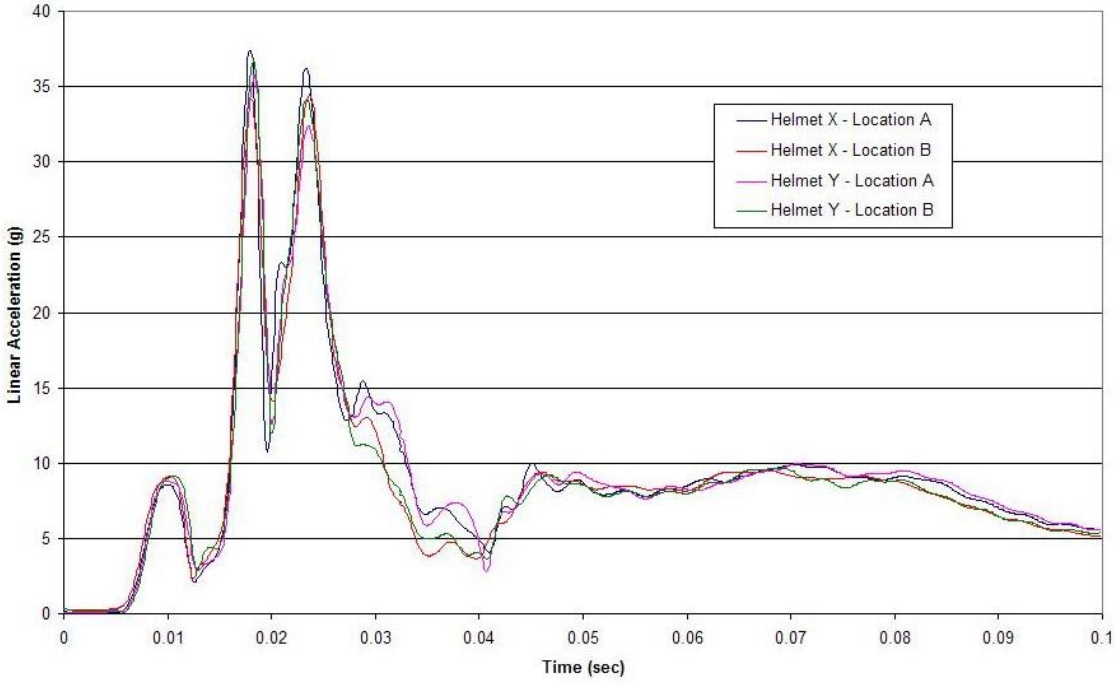


Figure A.7 - Linear acceleration time trace for Condition 3 at 77 Joules

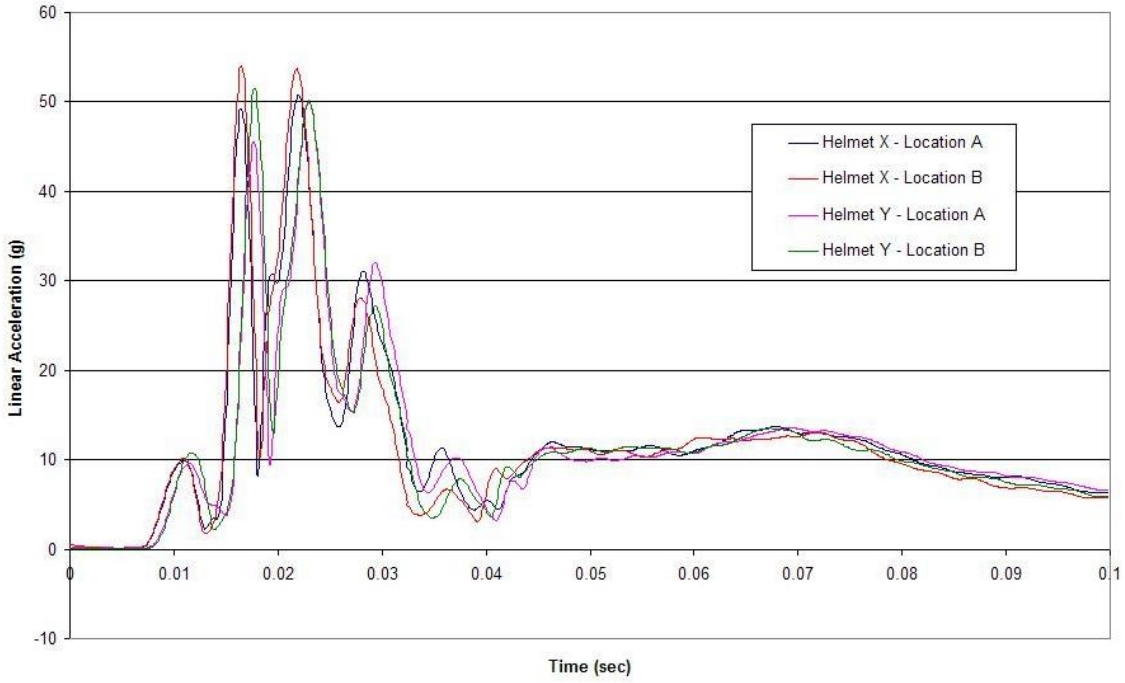


Figure A.8 - Linear acceleration time trace for Condition 3 at 121 Joules

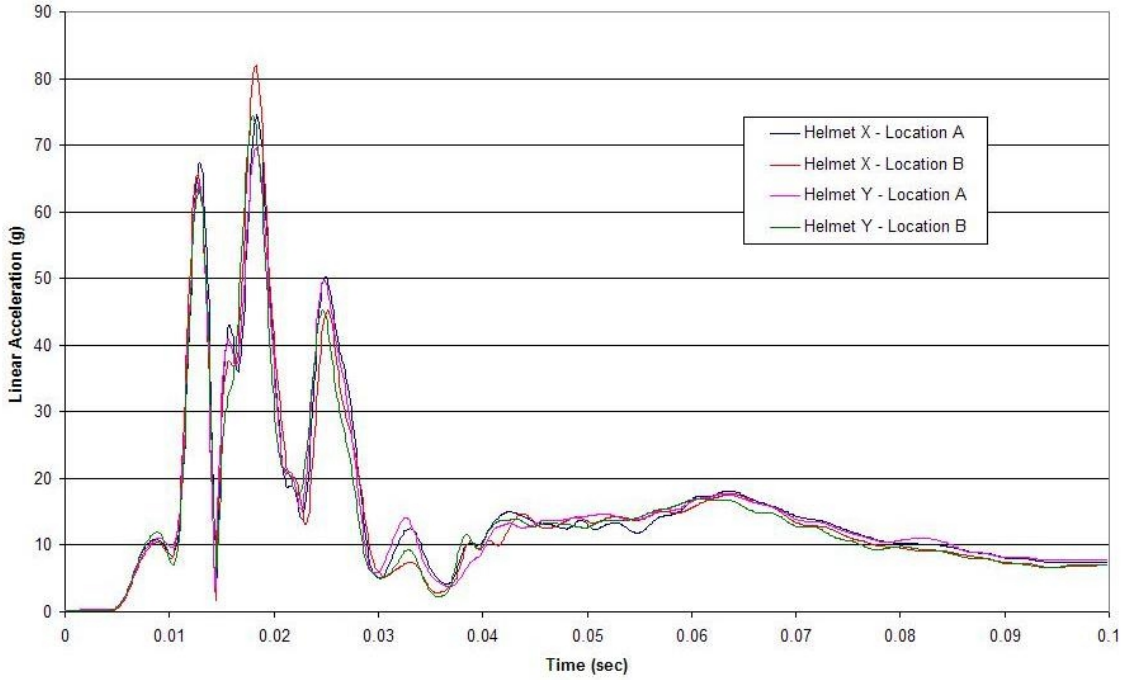


Figure A.9 - Linear acceleration time trace for Condition 3 at 160 Joules

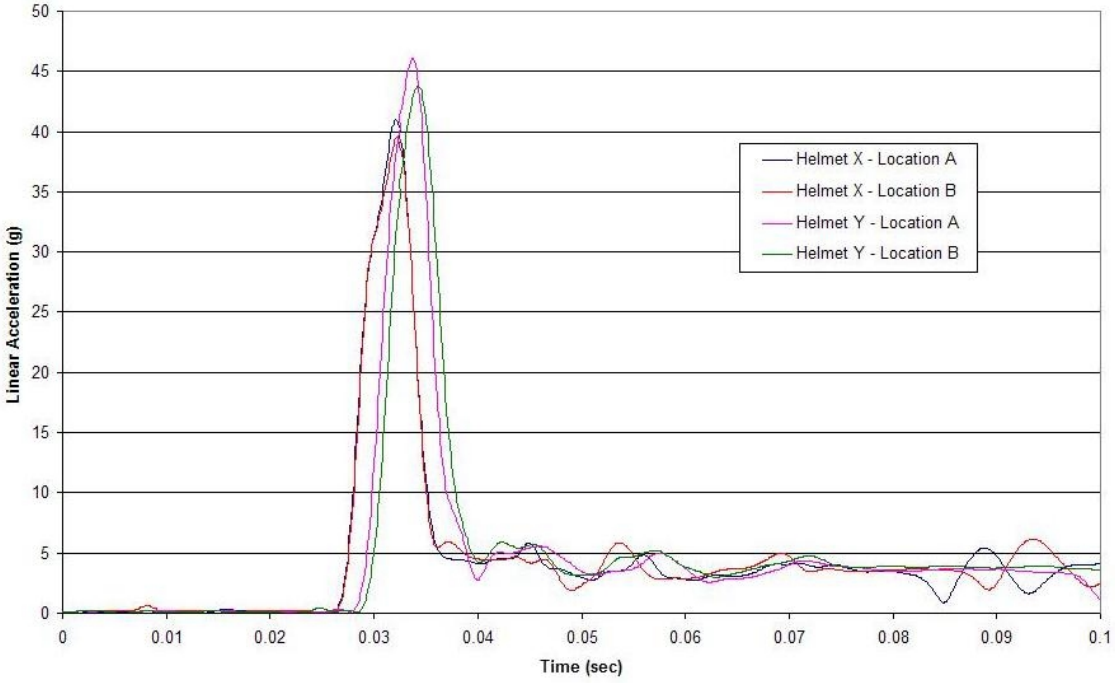


Figure A.10 - Linear acceleration time trace for Condition 4 at 77 Joules

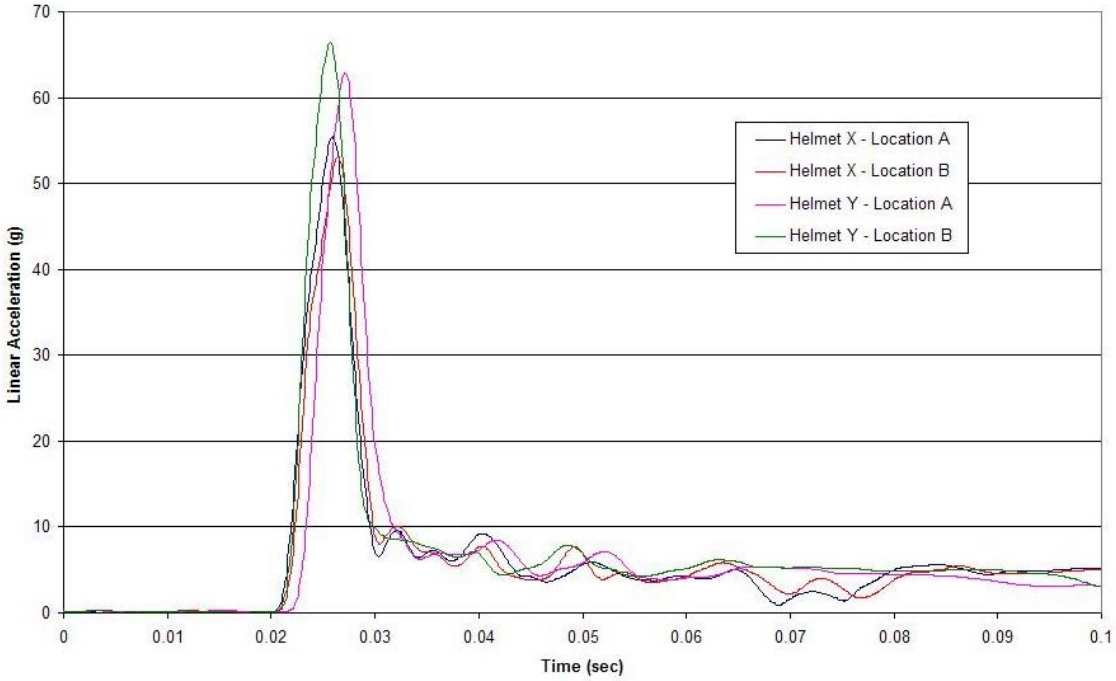


Figure A.11 - Linear acceleration time trace for Condition 4 at 121 Joules

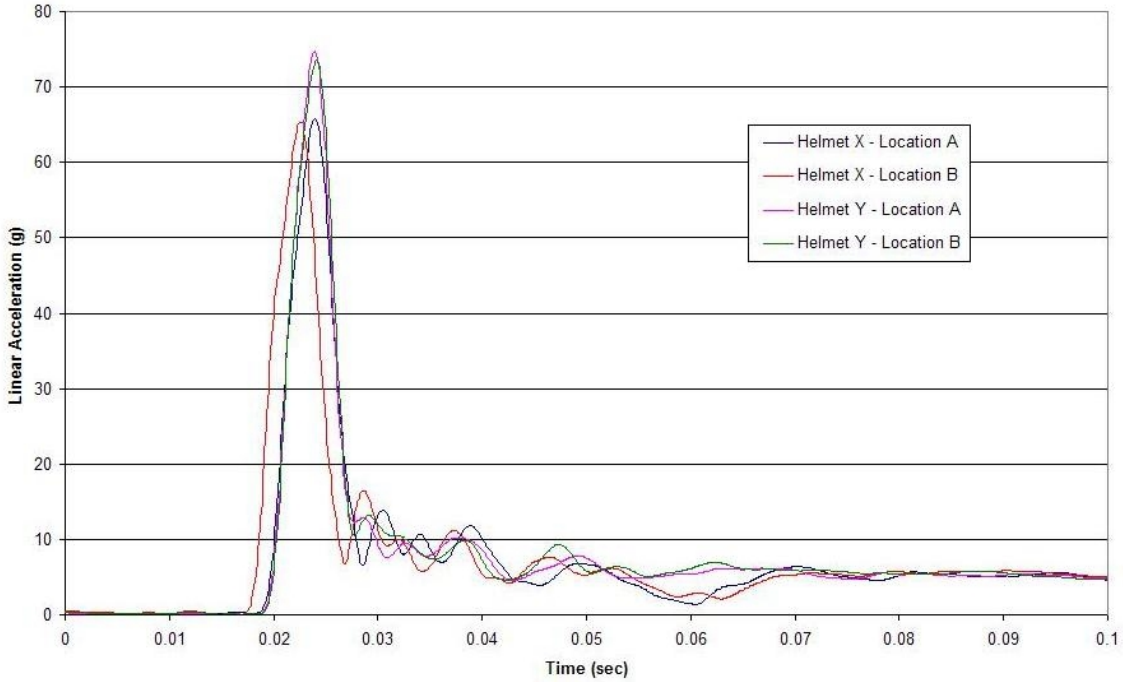


Figure A.12 - Linear acceleration time trace for Condition 4 at 160 Joules

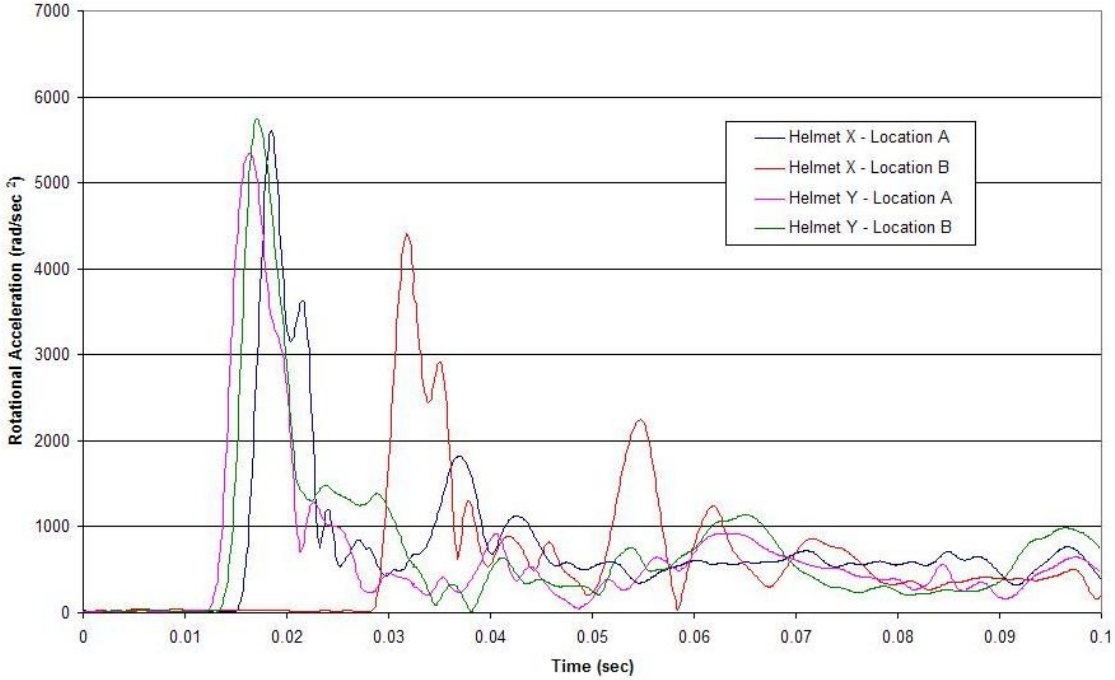


Figure A.13 - Rotational acceleration time trace for Condition 1 at 77 Joules

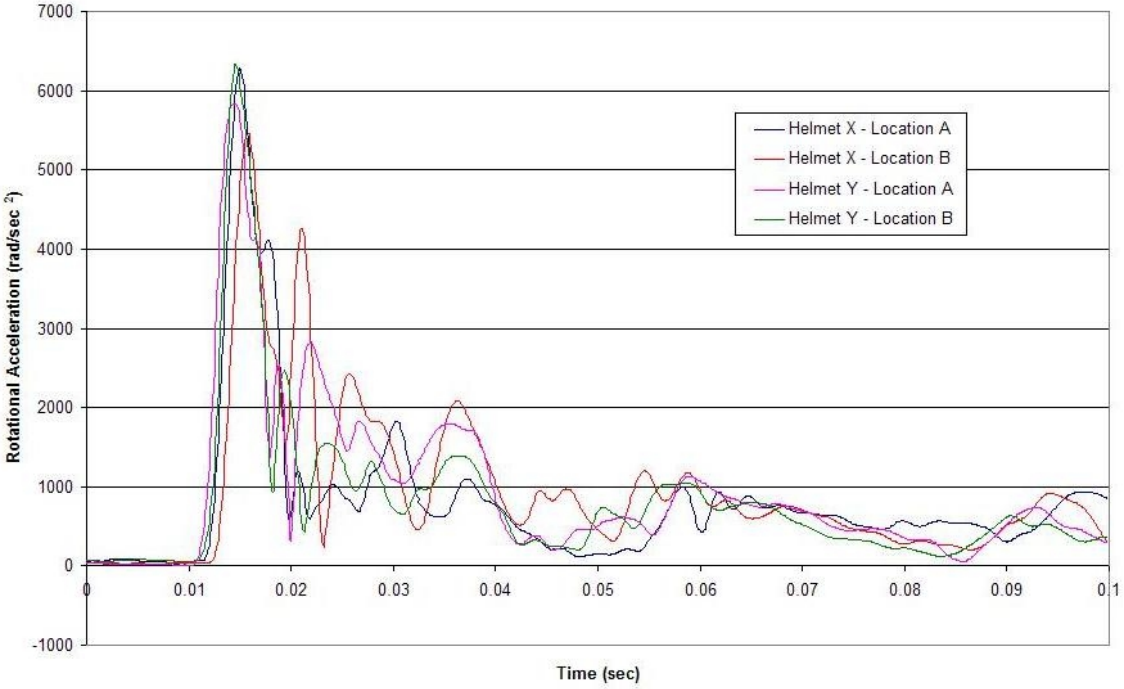


Figure A.14 - Rotational acceleration time trace for Condition 1 at 121 Joules

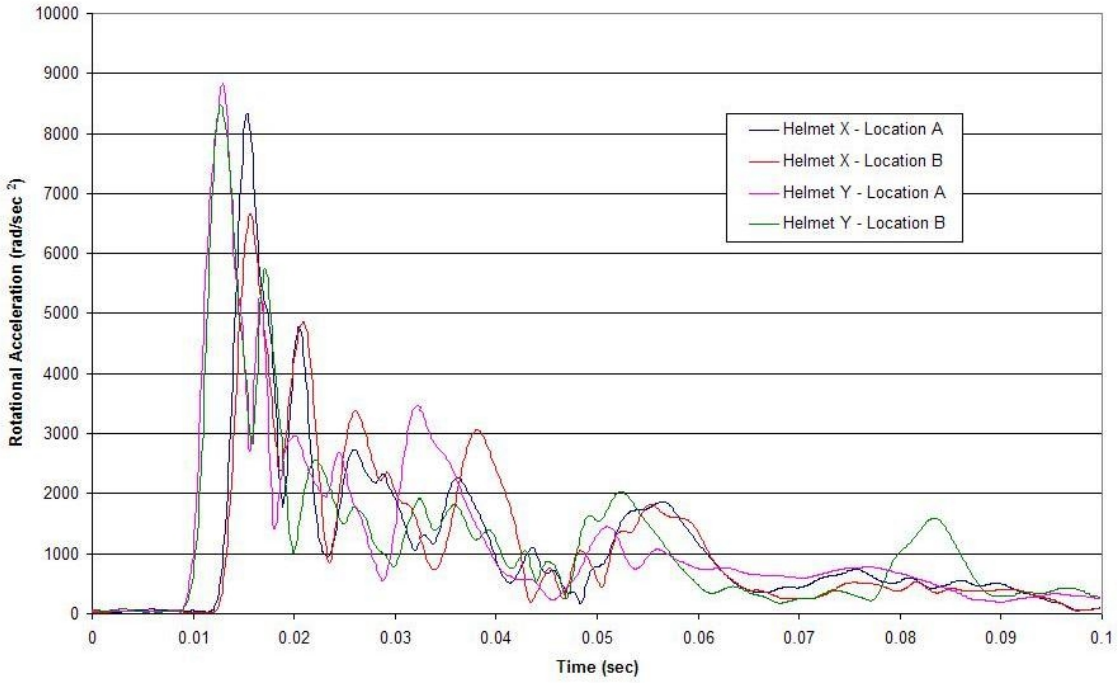


Figure A.15 - Rotational acceleration time trace for Condition 1 at 160 Joules

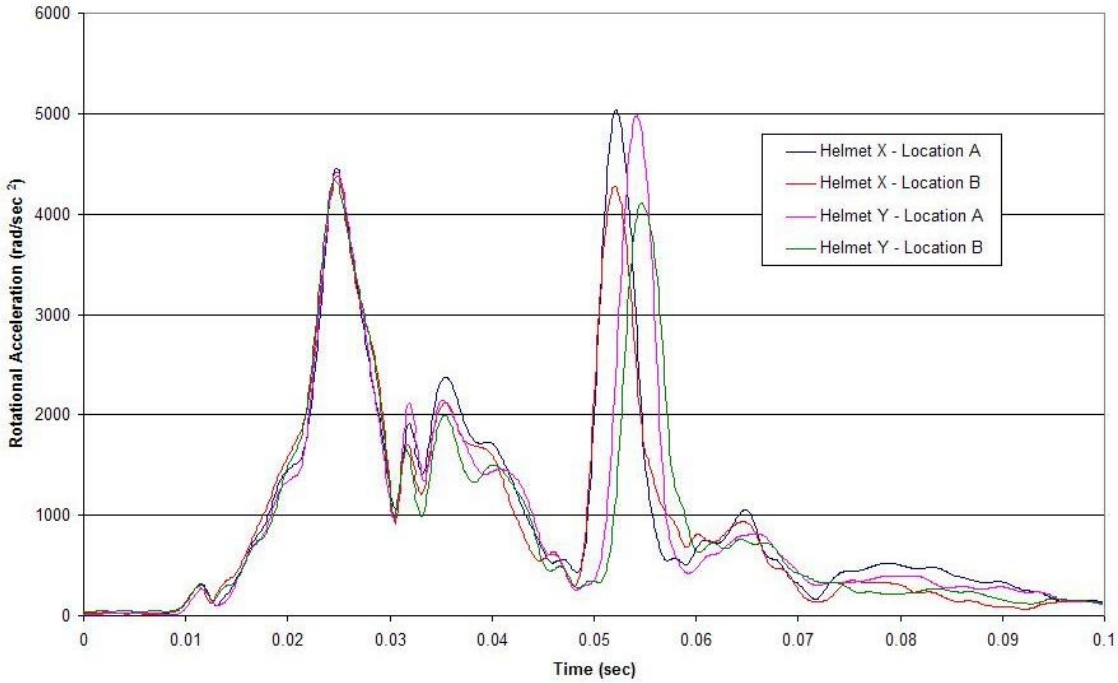


Figure A.16 - Rotational acceleration time trace for Condition 2 at 77 Joules

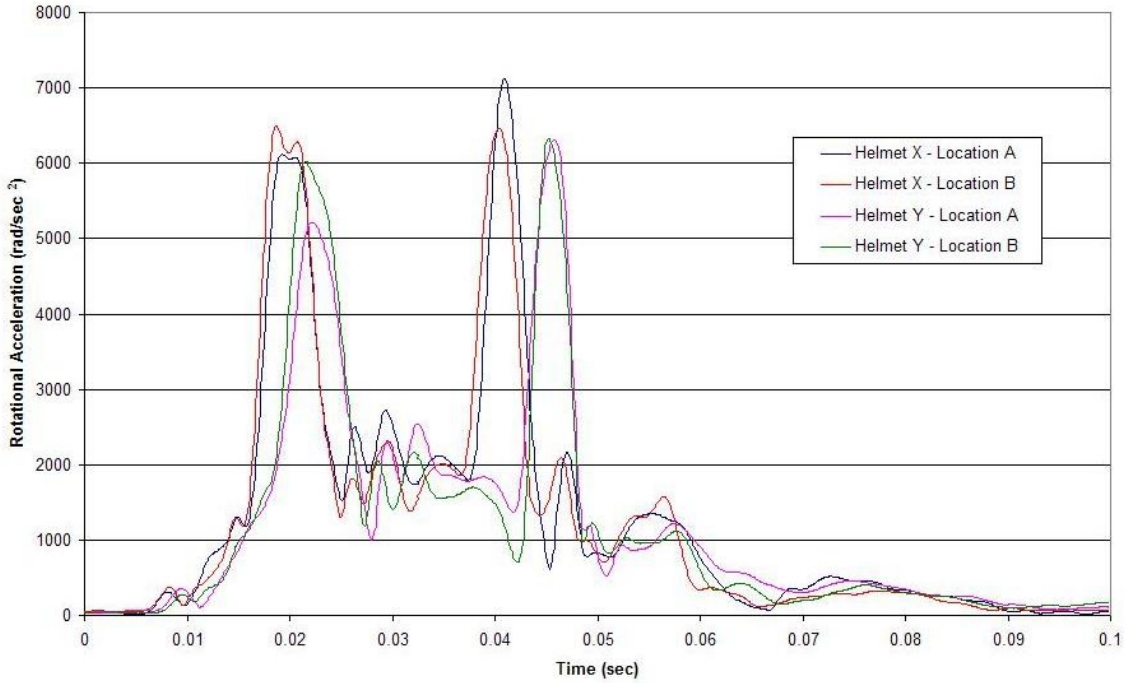


Figure A.17 - Rotational acceleration time trace for Condition 2 at 121 Joules

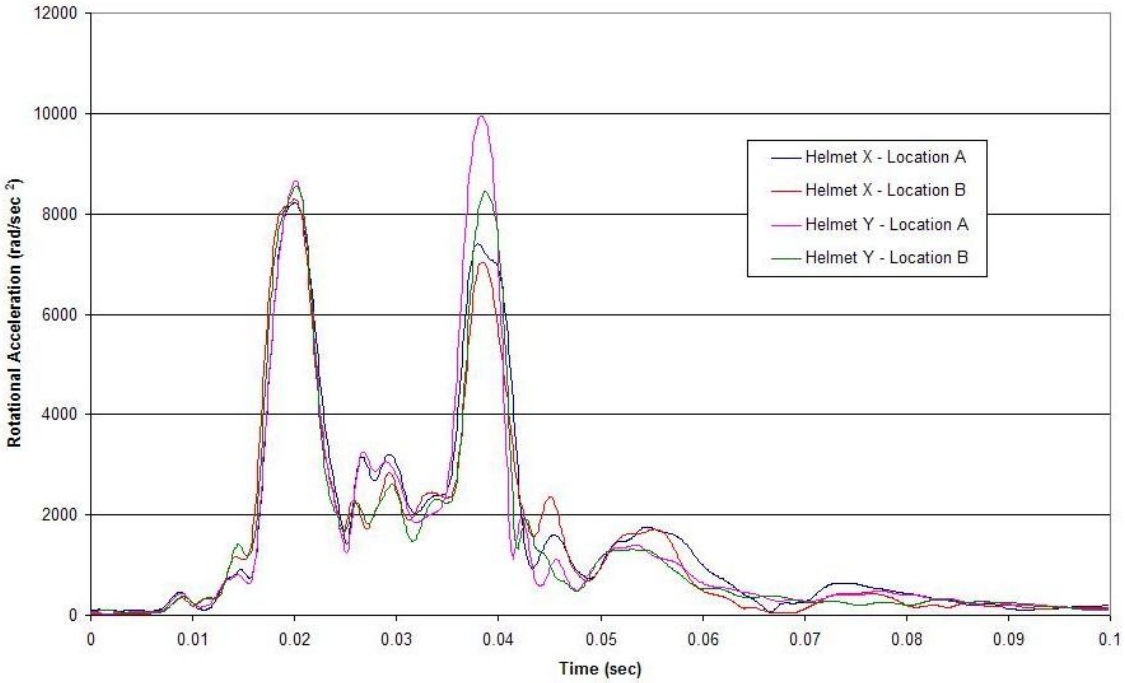


Figure A.18 - Rotational acceleration time trace for Condition 2 at 160 Joules

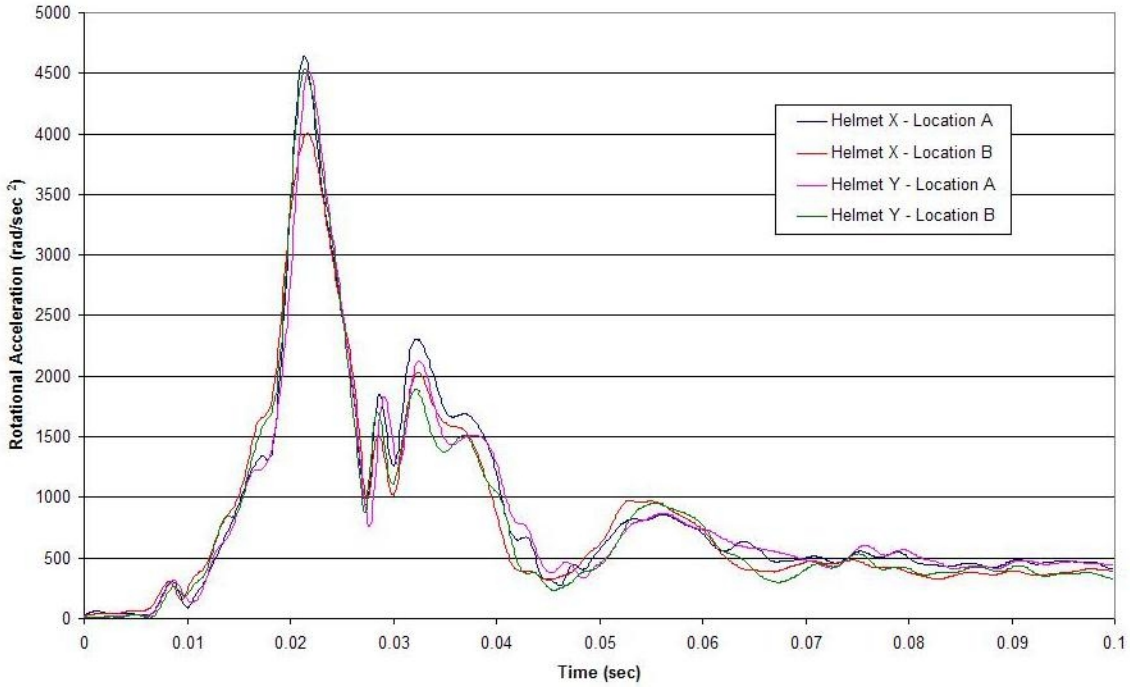


Figure A.19 - Rotational acceleration time trace for Condition 3 at 77 Joules

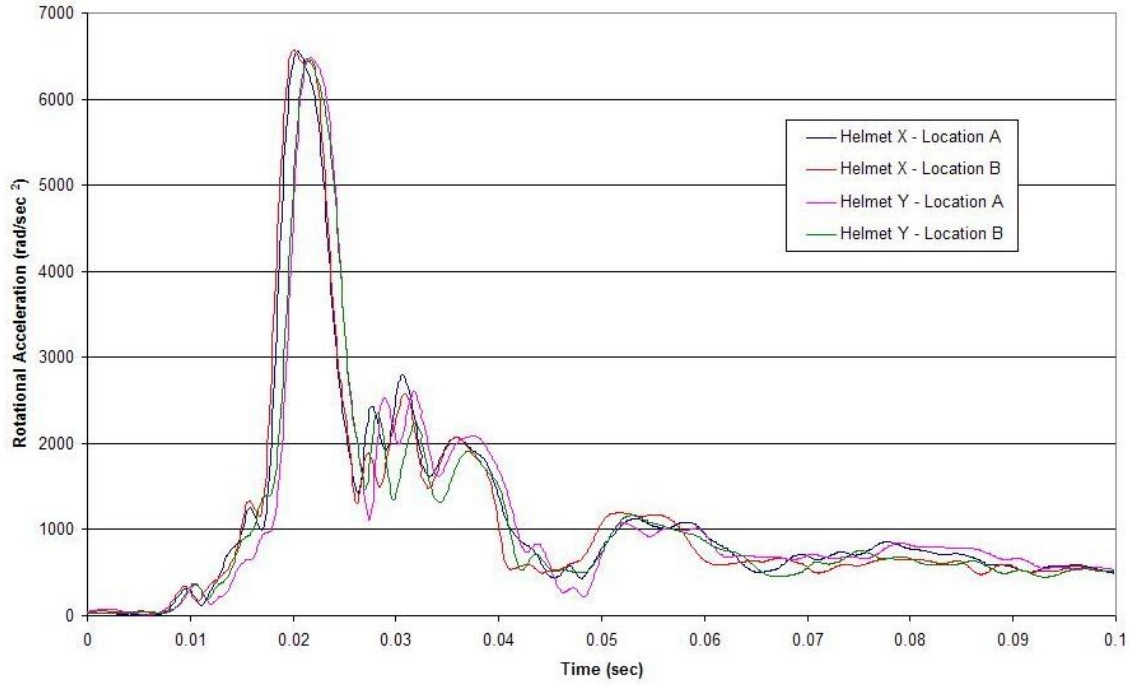


Figure A.20 - Rotational acceleration time trace for Condition 3 at 121 Joules

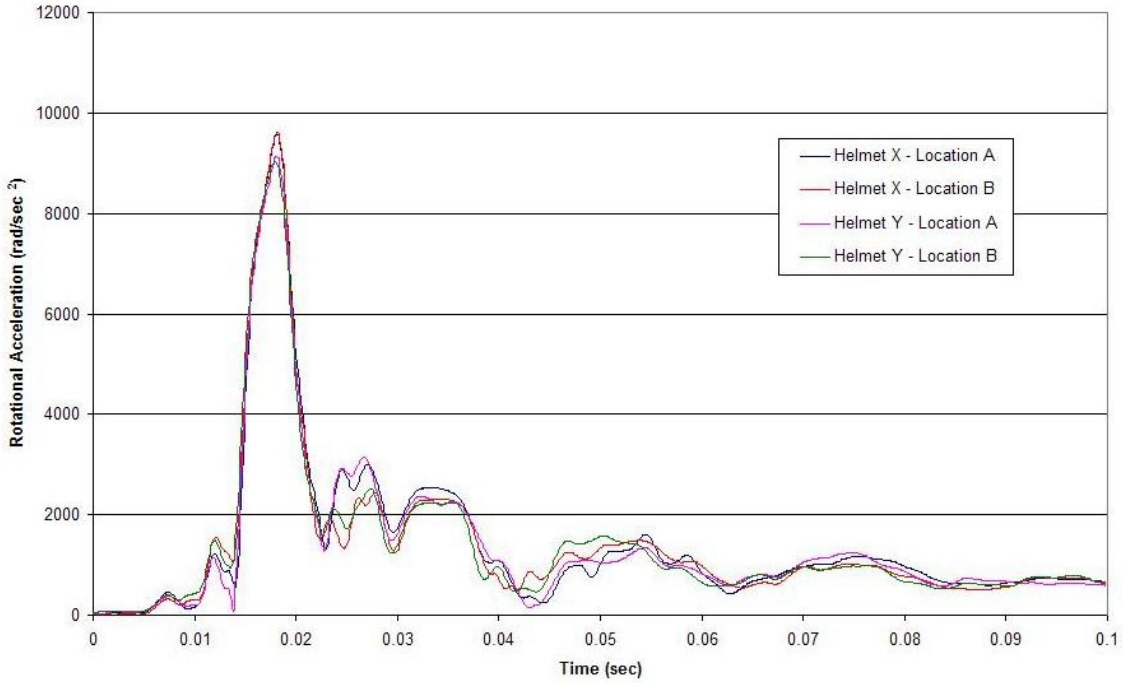


Figure A.21 - Rotational acceleration time trace for Condition 3 at 160 Joules

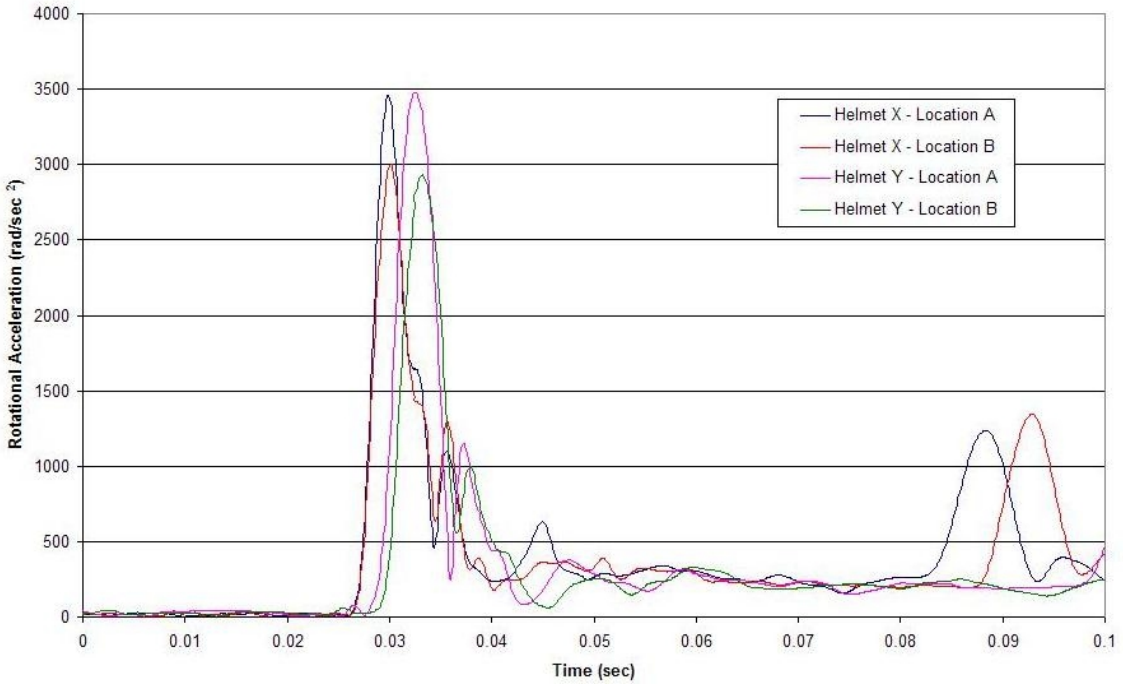


Figure A.22 - Rotational acceleration time trace for Condition 4 at 77 Joules

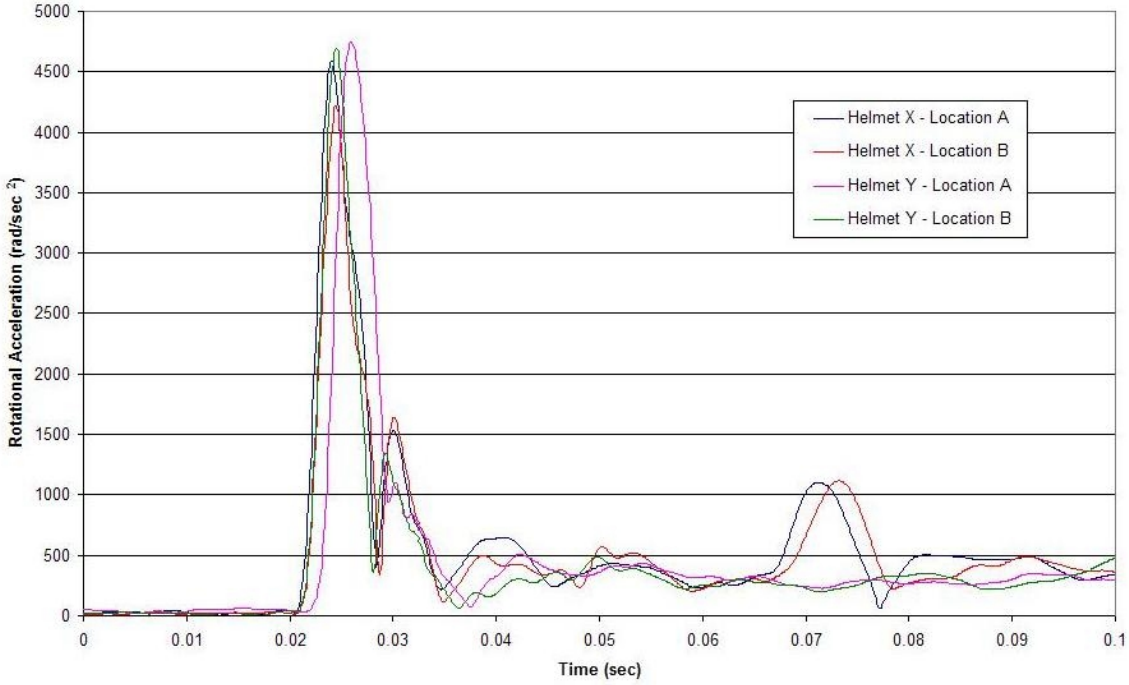


Figure A.23 - Rotational acceleration time trace for Condition 4 at 121 Joules

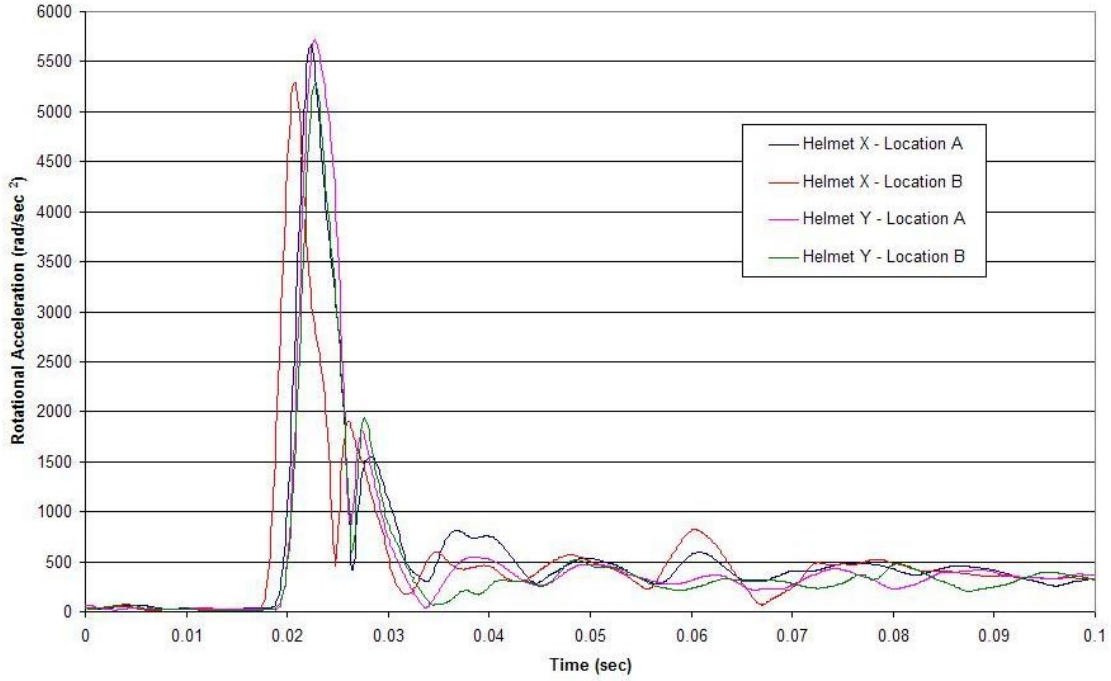


Figure A.24 - Rotational acceleration time trace for Condition 4 at 160 Joules

APPENDIX B

HIGH-SPEED VIDEO

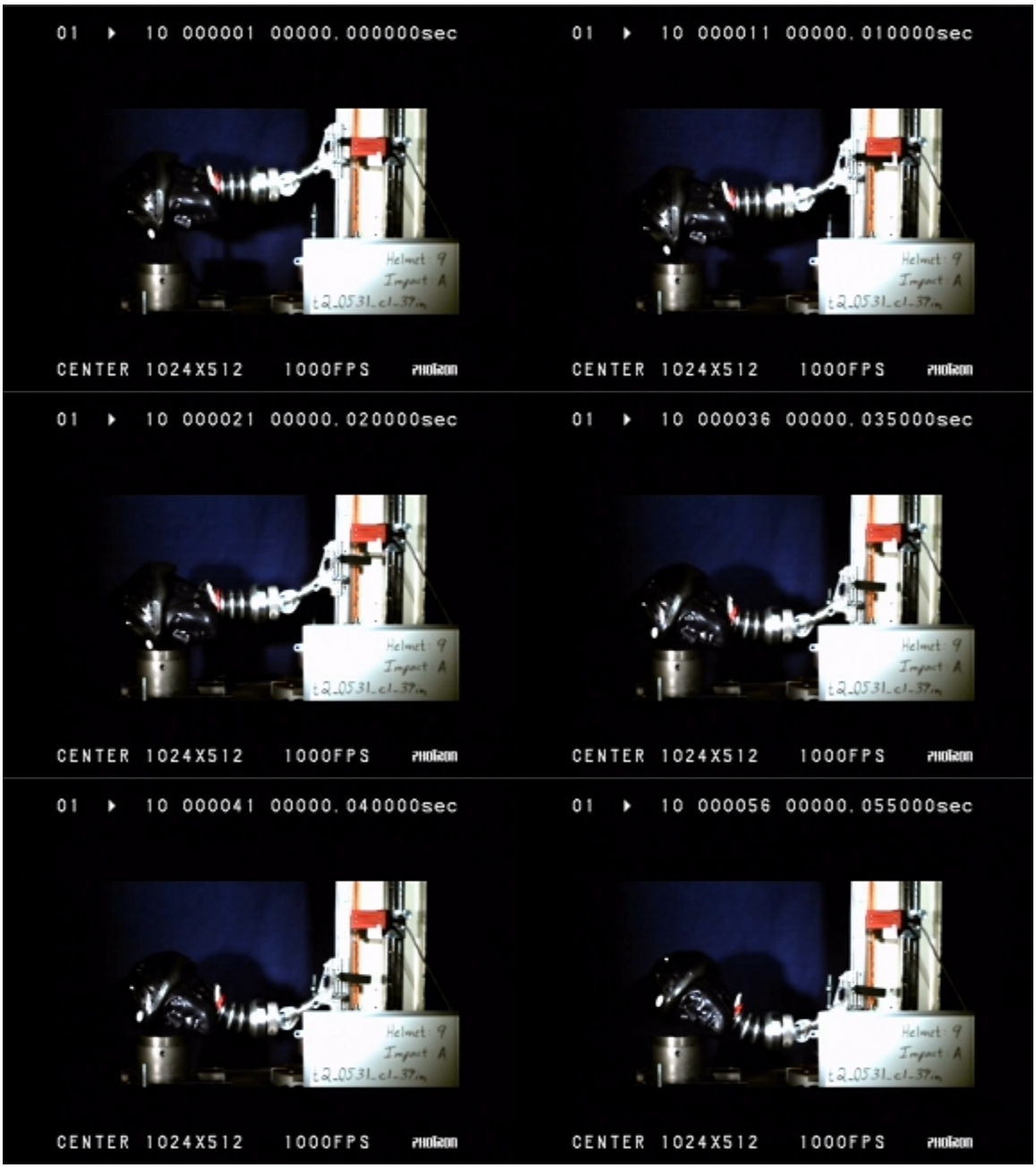


Figure B.1 - High-speed video screen captures of Condition 1 at 77 Joules



Figure B.2 - High-speed video screen captures of Condition 1 at 121 Joules

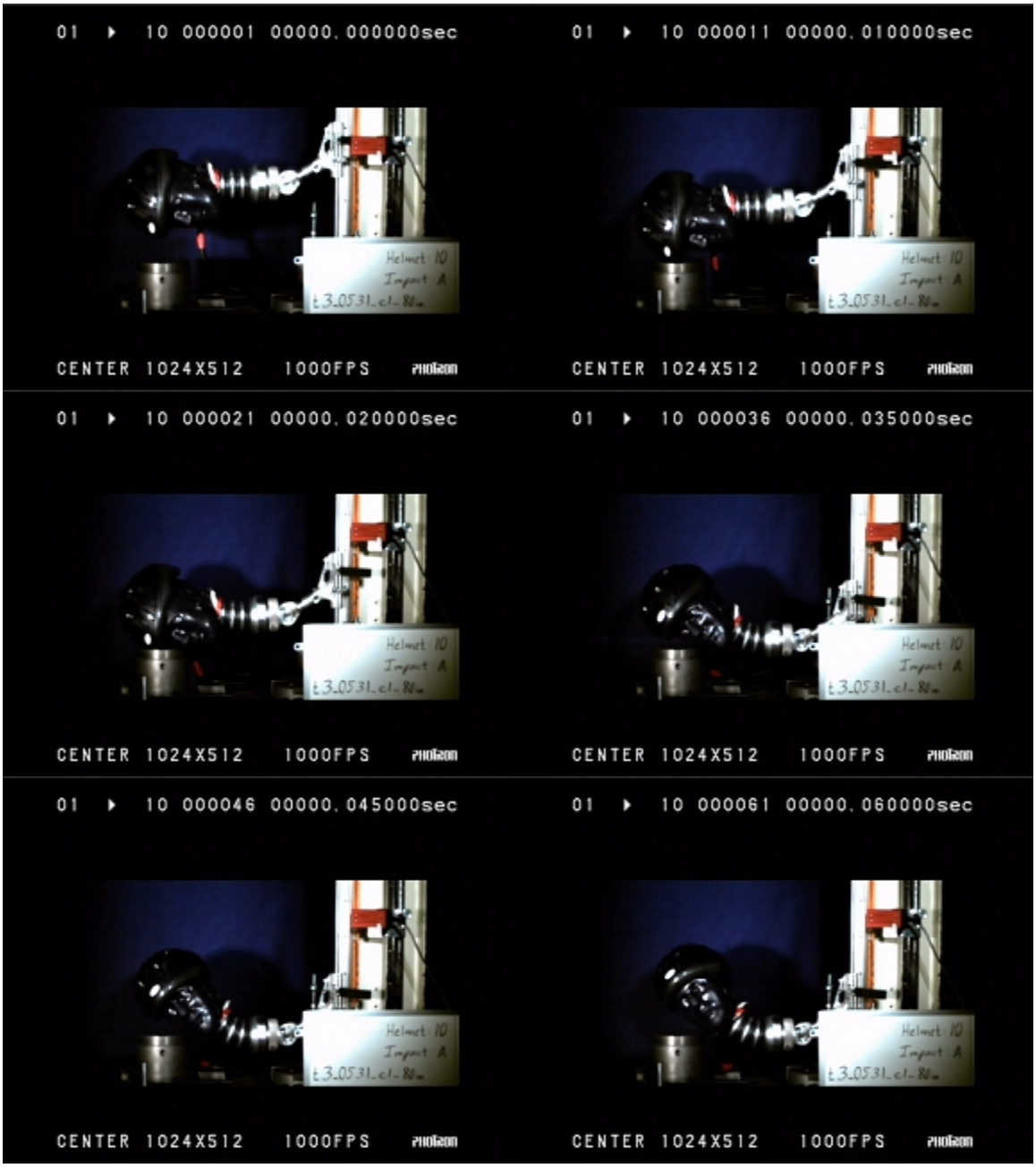


Figure B.3 - High-speed video screen captures of Condition 1 at 160 Joules

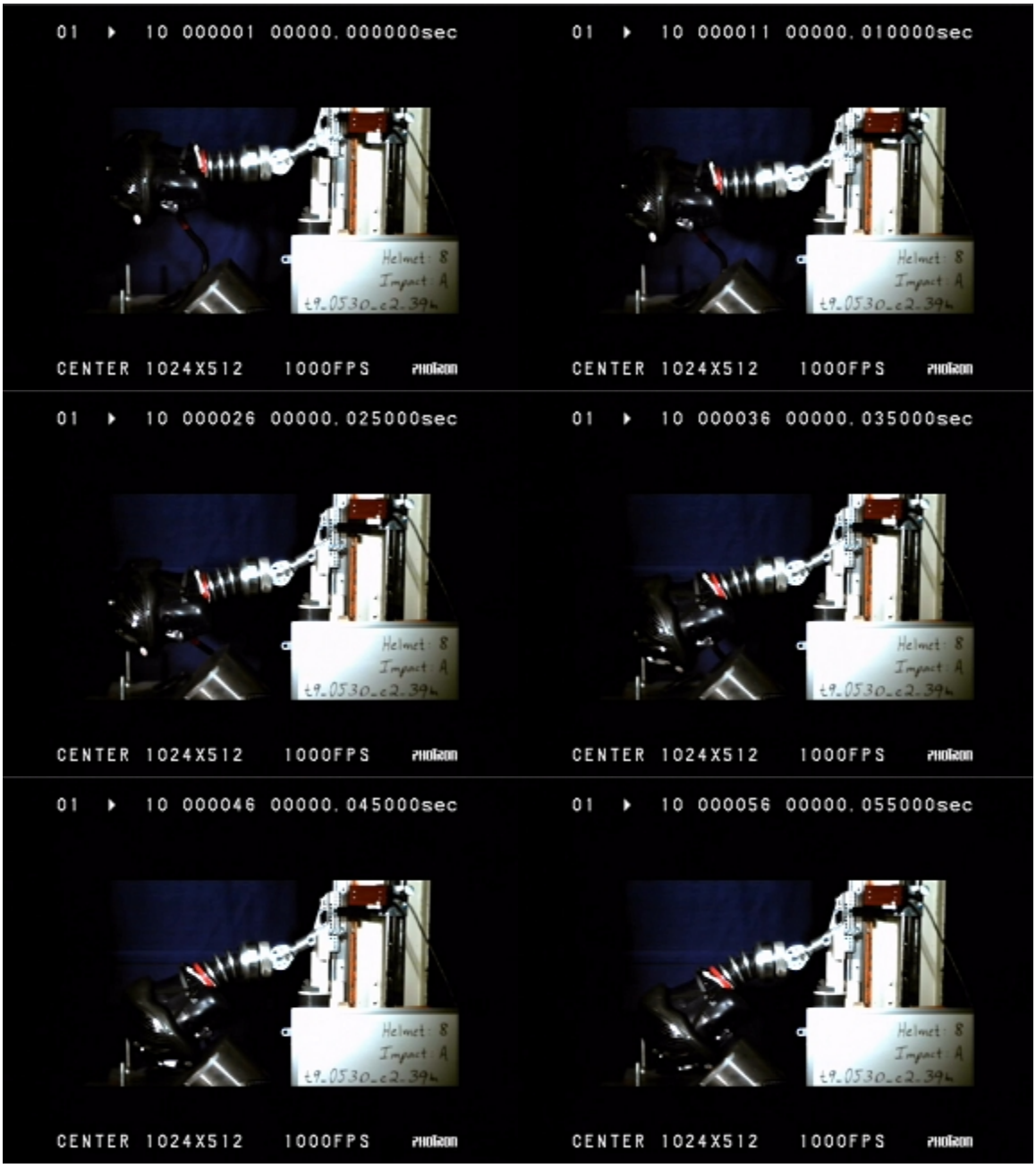


Figure B.4 - High-speed video screen captures of Condition 2 at 77 Joules



Figure B.5 - High-speed video screen captures of Condition 2 at 121 Joules



Figure B.6 - High-speed video screen captures of Condition 2 at 160 Joules



Figure B.7 - High-speed video screen captures of Condition 3 at 77 Joules



Figure B.8 - High-speed video screen captures of Condition 3 at 121 Joules



Figure B.9 - High-speed video screen captures of Condition 3 at 160 Joules



Figure B.10 - High-speed video screen captures of Condition 4 at 77 Joules

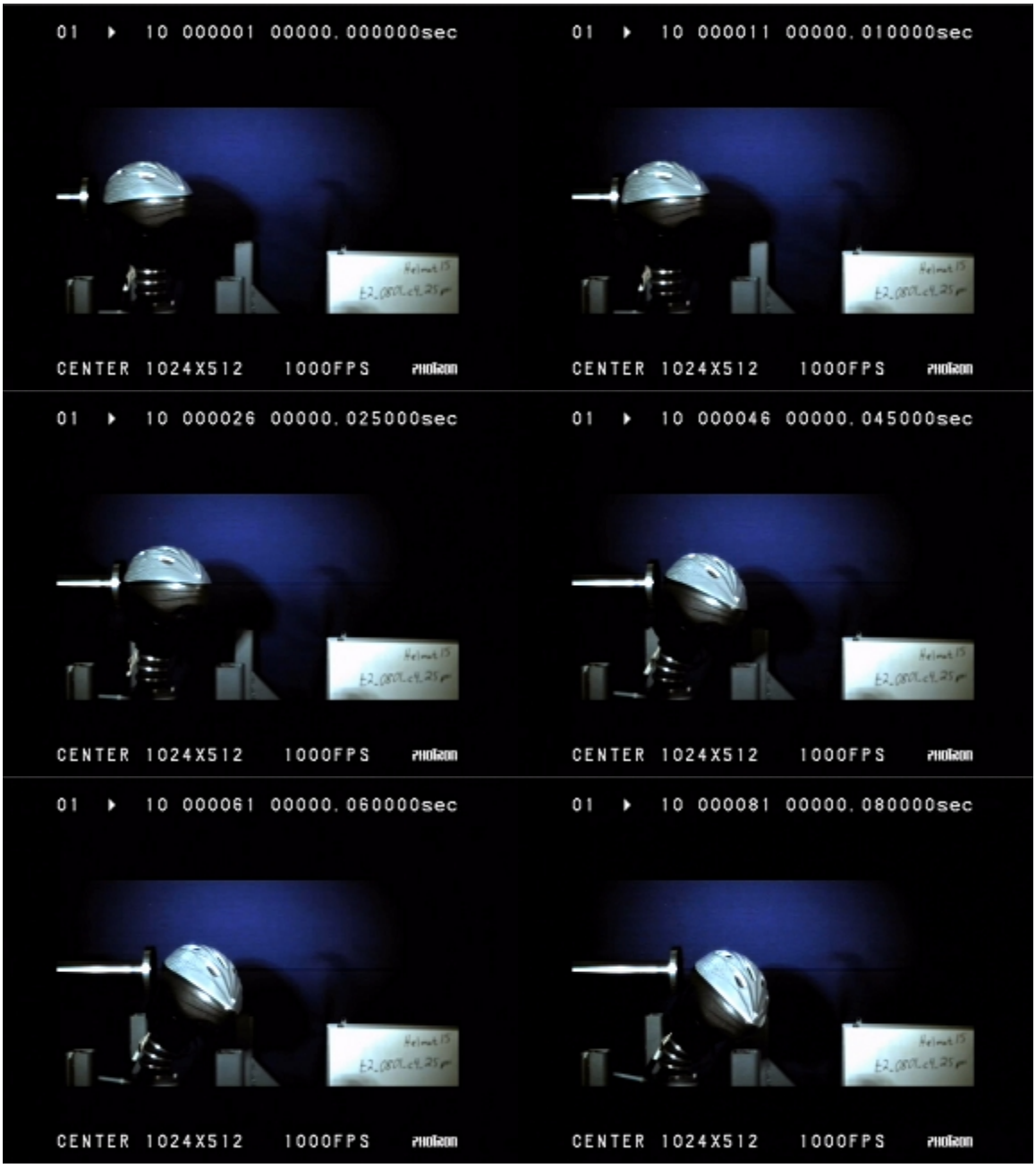


Figure B.11 - High-speed video screen captures of Condition 4 at 121 Joules



Figure B.12 - High-speed video screen captures of Condition 4 at 160 Joules

APPENDIX C

MISCELLANEOUS INFORMATION

EQUIPMENT INFORMATION

NOCSAE modified headform – S/N: RMM-9A

Hybrid III neck – S/N: 02021043A

Endevco DC Differential Voltage Amplifier – Model 136

National Instruments Connector Box – Model BNC-2090, S/N: D74ABE

National Instruments Data Acquisition (NI-DAQ) card – Model 6024E

Table C.1 - Information on Endevco 7264B-2000 Piezoresistive Accelerometers

Accelerometer	Position	Sensitivity (mV/g)	S/N
1	X-axis CG	0.2628	B34180
2	Y-axis CG	0.2735	B34269
3	Z-axis CG	0.2585	B34302
4	Z-axis Left	0.2252	B34205
5	X-axis Left	0.2404	B34211
6	Z-axis Front	0.2448	B34295
7	Y-axis Front	0.2607	B34306
8	X-axis Top	0.2800	B34240
9	Y-axis Top	0.2647	B34249

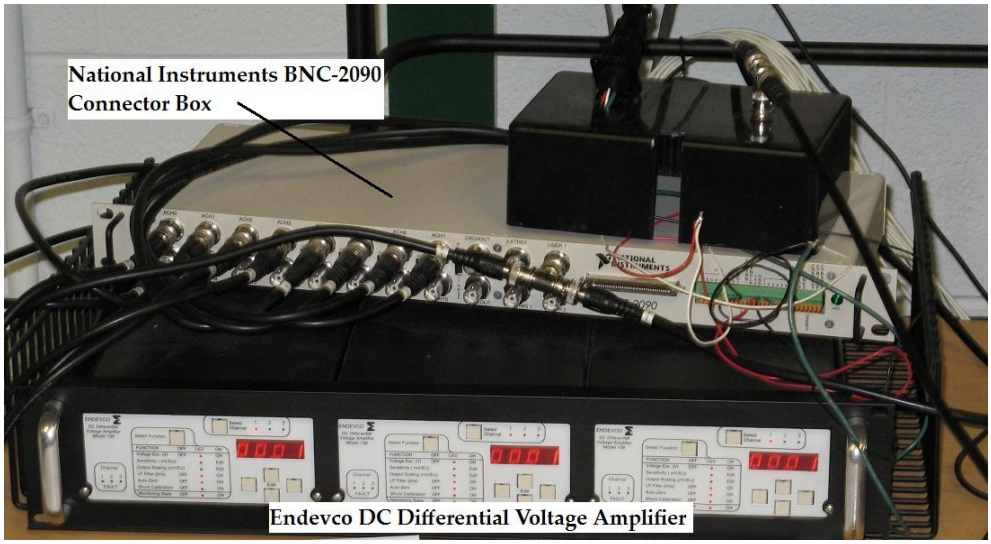


Figure C.1 - View of DC Differential Voltage Amplifier and Connector Box

Endevco

Model 7264B
Piezoresistive accelerometer

Features

- Mechanical overtravel stops
- Small size, rugged
- Crash and shock testing
- 500 g and 2000 g full scale ranges
- DC response - long duration transients



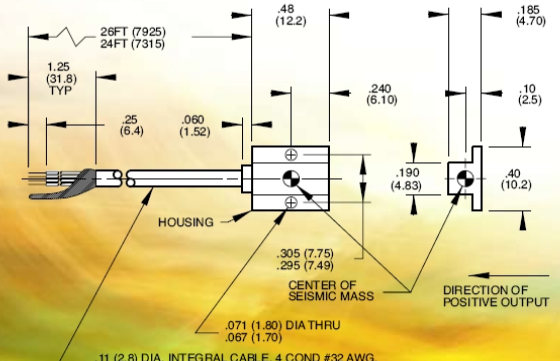
Description

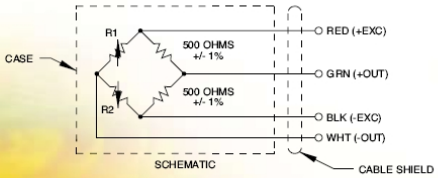
The Endevco® Model 7264B is a very low mass piezoresistive accelerometer weighing only 1 gram. This accelerometer is designed for crash testing, flutter testing, rough road testing and similar applications that require minimal mass loading and a broad frequency response. Used for shock testing of lightweight systems or structures, the Model 7264B accelerometer also meets SAEJ211 specifications for instrumentation for impact testing and SAEJ2570 specification for anthromorphic test device transducers.

The Model 7264B utilizes an advanced micromachined sensor which includes integral mechanical stops. This monolithic sensor offers improved ruggedness, stability and reliability over previous designs. The Model 7264B has minimum damping, thereby producing no phase shift over the useful frequency range. With a frequency response extending down to dc or steady state acceleration, this accelerometer is ideal for measuring long duration transients as well as short duration shocks.

The Model 7264B offers excellent linearity and a wide frequency response. Further, this accelerometer offers stable performance over the temperature range of -40°F to +200°F (-40°C to +93°C) and has a full bridge circuit with fixed resistors for shunt calibration. This accelerometer has a full scale output of 400 mV with 10 Vdc excitation (sensitivity of 0.80 mV/g for -500 and 0.20 mV/g for -2000). It is also available with less than 1% transverse sensitivity ("T" option) on special order.

Endevco Model 136 three-channel system, Model 4430A or Oasis 2000 computer-controlled system are recommended as signal conditioner and power supply.
U.S. Patents 4,498,229 and 4,605,919





STANDARD TOLERANCE
INCHES (MILLIMETERS)
.XX = +/- .02 (.X = +/- .5)
.XXX = +/- .010 (.XX = +/- .25)

MEGGiTT
smart engineering for
extreme environments

*obtained from www.endevco.com

Figure C.2 - Endevco 7264B acclerometer data sheet (page 1)

Model 7264b
Piezoresistive Accelerometer

Endevco

SPECIFICATIONS

CERTIFIED PERFORMANCE: All values are typical at 75°F (+24°C), 100 Hz and 10 Vdc excitation unless otherwise specified. Calibration data, traceable to the National Institute of Standards (NIST), is supplied.

	Units	7264B-500	7264B-2000
RANGE	g	±500	±2000
SENSITIVITY (at 100 Hz)	mV/g Typ	0.80	0.20
	(Min)	(0.40)	(0.15)
AMPLITUDE RESPONSE			
±5%	Hz	0 to 3000	0 to 5000
±2% "G" option	Hz	0 to 2000	0 to 3500
MOUNTED RESONANCE FREQUENCY	Hz	17 000	28 000
DAMPING RATIO	Typ	0,005	0,005
NON-LINEARITY AND HYSTERESIS			
(% of reading, to full range)	% Max	±1	±1
TRANSVERSE SENSITIVITY [1]	% Max	3	3
ZERO MEASURAND OUTPUT	mV Max	±25	±25
THERMAL ZERO SHIFT			
From 0°F to +150°F (-18°C to +66°C), ref. 75°F(24°C)	mV Max	±25	±25
THERMAL SENSITIVITY SHIFT	%/°F Typ	- 0,06	- 0,06
From 0°F to +150°F (-18°C to +66°C), ref. 75°F(24°C)	%/°C Typ	- 0,10	-0,10
WARM-UP TIME	ms Max	1, 15 μ sec typical	1, 15 μ sec typical
BASE STRAIN SENSITIVITY			
(Per ISA 37.2 @ 250 μ strain)	Equiv. g's	< 0.1	< 0.1
MECHANICAL OVERTRAVEL STOPS	g's	1500 g typical, 750 g minimum	5000 g typical, 2500 g minimum

ELECTRICAL	
EXCITATION [2]	10.0 Vdc (5Vdc and 2Vdc optional)
INPUT RESISTANCE [3]	300 to 900 ohms
OUTPUT RESISTANCE [3]	400 to 1600 ohms
FIXED RESISTORS	500 ohms ±1%
INSULATION RESISTANCE	100 megohms minimum at 100 Vdc; leads to case, leads to shield, shield to case

PHYSICAL	
CASE, MATERIAL	Blue Anodized aluminum alloy
ELECTRICAL, CONNECTIONS	Integral cable, four conductor No. 32 AWG Teflon® insulated leads, braided shield, silicone jacket
MOUNTING/TORQUE	Holes for two 0-80 mounting screws/3 lbf-in (0.3 Nm)
WEIGHT	1 gram (cable weighs 9 grams/meter)

ENVIRONMENTAL		
ACCELERATION LIMITS (in any direction)		
Static	5000 g	10 000 g
Sinusoidal Vibration	1000 g pk below 3kHz	1000 g pk below 5kHz
Shock (half-sine pulse duration)	5000 g, 300 μsec or longer	10 000 g, 200 μsec or longer
TEMPERATURE		
Operating	-40°F to +200°F (-40°C to +93°C)	
Storage	-65°F to +250°F (-54°C to +121°C)	
HUMIDITY	Unit is epoxy sealed	
ALTITUDE	Unaffected	

CALIBRATION DATA SUPPLIED [5]	
SENSITIVITY (at 100 Hz and 10 g pk)	mV/g
FREQUENCY RESPONSE	20 Hz to 3000 Hz, % deviation reference 100 Hz; dB plot continued from 3000 to 30 000 Hz for 7264B-500: 20 Hz to 5000 Hz, % deviation reference 100 Hz; dB plot continued from 5000 to 30 000 Hz for 7264B -2000
ZERO MEASURAND OUTPUT	mV
MAXIMUM TRANSVERSE SENSITIVITY	% of sensitivity
INPUT AND OUTPUT RESISTANCE	Ohms

INCLUDED ACCESSORIES

EHM35	(1) HEX WRENCH
EHW196	(2) SIZE-0 FLAT WASHERS
EH492	(2) 0-80 X 3/16 INCH SOCKET HEAD CAP SCREWS
16385-2	SAFETY SLEEVE [4]

OPTIONAL ACCESSORIES

24328 -1,-2,-3	4 CONDUCTOR SHIELDED CABLE
7964A	TRIAXIAL MOUNTING BLOCK

NOTES

1. 1% transverse sensitivity available as "T" option.
2. Lower excitation voltages may be used but should be specified at time of order to obtain best calibration.
3. Measured at approximately 1 Vdc. Bridge resistance increases with applied voltage due to heat dissipation in the strain gage elements.
4. The safety sleeve should be kept on unit when not in use to prevent possible handling damage.
5. Maintain high levels of precision and accuracy using Endevco's factory calibration services. Call Endevco's inside sales force at 800-982-6732 for recommended intervals, pricing and turn-around time for these services as well as for quotations on our standard products.

Continued product improvement necessitates that Endevco reserve the right to modify these specifications without notice. Endevco maintains a program of constant surveillance over all products to ensure a high level of reliability. This program includes attention to reliability factors during product design, the support of stringent Quality Control requirements, and compulsory corrective action procedures. These measures, together with conservative specifications have made the name Endevco synonymous with reliability.

APPLIES TO CALIFORNIA FACILITY

©ENDEVCO CORPORATION. ALL RIGHTS RESERVED 30700 RANCHO VIEJO ROAD, SAN JUAN CAPISTRANO, CA 92675 USA
(800) 982-6732 • (949) 493-8181 fax (949) 661-7231 • www.endevco.com • Email: applications@endevco.com

0805

MEGGiTT
smart engineering for extreme environments

*obtained from www.endevco.com

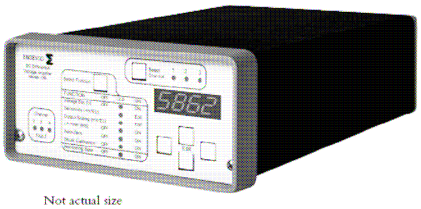
Figure C.3 - Endevco 7264B acclerometer data sheet (page 2)

DC Amplifier

ENDEVCO MODEL 136

Model 136

- **Three-Channel DC Differential Voltage Amplifier**
- **200 kHz Bandwidth (-3dB Corner)**
- **Auto-Zero and Shunt Calibration**
- **Gain Range 0 to 1000**
- **Four Selectable Excitation Voltage Levels**
- **RS-232 Serial Interface**
- **12 VDC Power Option**
- **Built-in 4-Pole Butterworth Low-Pass Filter**



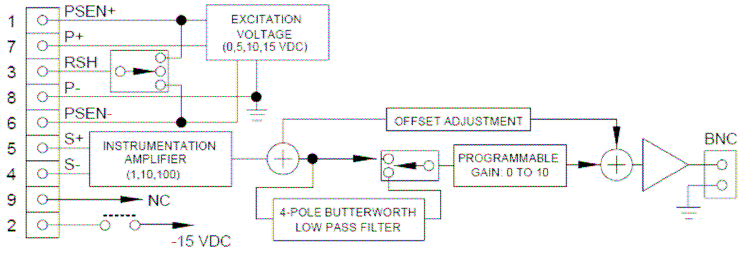
Not actual size

DESCRIPTION

The ENDEVCO® Model 136 is a three-channel, DC amplifier that is manually or computer programmable. Manual control is accomplished at the front panel by means of a "Select Channel" push-button, three (3) "Channel LEDs", one "Select Function" push-button, five "Function LEDs", a four character LED display, showing the state of each function/channel, and four "Edit" push-buttons to change the entries in the LED display. There are three LEDs used as fault status indicators for the auto zero function. Computer control is accomplished using the standard RS-232 port and optional Application Software.

There are two modes of operation, Normal and Programming/Setup. Both modes of operation utilize the front panel LED Display. In the Normal Mode, there are two states, Monitoring Mode and No-Monitoring. In the Monitoring Mode the LED display indicates the RMS reading of the signal present at the output of the selected channel. The Non-Monitoring Mode turns off the LED display for lower noise applications and to minimize power consumption. In the Programming Mode, the unit is ready for manual programming or editing of existing channel setups. The unit will automatically return to the Normal Mode of operation after 20 seconds of inactivity of the front panel or after pressing the "Select Function" push-button while the "Monitoring State" function LED is flashing.

The rear panel contains (on a per-channel basis) a BNC output connector, a 9-pin "D" input connector, the RS-232 connector, and the input power connector. Three Model 136 units may be configured in a 19-inch rack mount adapter. The standard unit is powered by 90-264 VAC, 50/60 Hz. The -1 option is powered by 9 to 18 VDC, making it ideal for portable use or for automobile test applications.



Technical Illustration

MEGGITT

CERTIFIED ISO 9001

APPLIES TO CALIFORNIA FACILITY

ENDEVCO

***obtained from www.endevco.com**

Figure C.4 - Endevco model 136 voltage amplifier data sheet (page 1)

ENDEVCO MODEL 136

DC Amplifier

SPECIFICATIONS

INPUTS

INPUT IMPEDANCE	1 Meg Ohm minimum
INPUT RANGE: DIFFERENTIAL	0 to ± 10 VDC or peak VAC, 9 pin "D" connector for each bridge sensor
COMMON MODE	± 10 VDC or pk VAC, inclusive of signal 50 Vpk without damage
COMMON MODE REJECTION	70 dB minimum, 200Ω or less input imbalance, DC to 60kHz
INPUT IMBALANCE ADJUSTMENT	± 100 mVDC, 100 ≤ gain ≤ 1000 ± 1 VDC , 10 ≤ gain ≤ 100 ± 10 VDC, 0 ≤ gain ≤ 10

OUTPUTS

AC/DC VOLTAGE	Single ended, short circuit protected
OUTPUT IMPEDANCE	0.2 Ohm maximum
LINEAR OUTPUT	10 Vpk
CURRENT OUTPUT	10 mA, minimum
OUTPUT DC BIAS STABILITY TEMP.	± 5 µV/°C RTI or ± 0.1 mV/°C RTO
OUTPUT DC BIAS STABILITY TIME	± 20 µV RTI or ± 5 mV RTO, whichever is greater, for 24 hours, after a 1 hour warmup
EXCITATION VOLTAGE	0, 5.0, 10.0, or 15.0 VDC, Front Panel or computer selected; 1 selection for all 3 channels.
EXCITATION VOLTAGE ACCURACY	± 1%
EXCITATION CURRENT	30 mA maximum, short circuit protected
NOISE & RIPPLE	1 mVRMS maximum, 10 Hz to 50 kHz, with 1 kOhm load

TRANSFER CHARACTERISTICS

GAIN	
RANGE	Programmable from 0 to 1000
RESOLUTION	0.0025, 0 ≤ gain ≤10 0.025,10 ≤ gain ≤ 100 0.25, 100 ≤ gain ≤ 1000
ACCURACY	± 0.5% of full scale maximum, DC to 1 kHz, filters disabled
LINEARITY	0.1% of full scale, best fit straight line at 1 kHz reference
STABILITY	± 0.2% of full scale, 0°C to + 50°C
NOISE	20 µVRMS RTI plus 1 mVRMS RTO, whichever is greater, DC to 50 kHz, with a 1k Ohm source resistance unit in Non-Monitoring State, 10 kHz internal lowpass filter enabled
BROADBAND FREQUENCY RESPONSE	DC to 200 kHz -3dB referenced to 1 kHz
FILTER CHARACTERISTICS	
FILTER TYPE	4-Pole Butterworth
CORNER FREQUENCY (-3 dB)	10 kHz ±12 % (other corners available by changing internal module 31875: 10 Hz to 80 kHz)
CROSSTALK BETWEEN CHANNELS	80 dB RTI

POWER REQUIREMENTS

VOLTAGE	Standard unit: 90-264 VAC 50 to 60 Hz; -1 Option: 9-18 VDC
POWER DISSIPATION	10 Watts typical
ISOLATION	No isolation channel to channel or signal ground to caseground

PHYSICAL CHARACTERISTICS

DIMENSIONS	5.57" X 2.52" X 12"
WEIGHT	4 lbs typical
CASE MATERIAL	Black Aluminum Cover, Medium Grey Plastic Bezel

ACCESSORIES

IM136	INSTRUCTION MANUAL
EW599	POWER CORD
31875-1000	10 KHZ, 4-POLE, BUTTERWORTH LOWPASS FILTER MODULE

OPTIONS

35933	APPLICATION SOFTWARE
EJ847	RJ11 (6X4) STRAIGHT WIRED INLINE COUPLER
EW1077	RJ11 4 CONDUCTOR MODULAR FLAT CABLE, STRAIGHT WIRED, 2 FEET LONG
EW1027	RJ11 4 CONDUCTOR MODULAR FLAT CABLE, STRAIGHT WIRED, 7 FEET LONG

OPTIONS CONTINUED

EJ807	SERIAL DB9F/RJ11 ADAPTER
EJ822	MODULAR SPLITTER ADAPTER, 1 (6X4) MALE TO 3 (6X4) FEMALE
136-1	9 - 18 VDC INPUT POWER OPTION
31875-XXXX	LOWPASS FILTER MODULES (SEE 31875 DATA SHEET)
31979	RACK MOUNT KIT
EHM1471	BLANK PANEL
EHM1413	DESKTOP DC POWER SUPPLY
EHM1409	AUTOMOTIVE POWER PLUG
29719-2	DB9M CONNECTOR KIT

WARNING! USE OF RJ11 CABLE OTHER THAN THAT SPECIFIED HEREIN WILL CAUSE CATASTROPHIC FAILURE OF THE UNIT.

Notes

Maintain high levels of precision and accuracy using Endevco's factory calibration services. Call Endevco's inside sales force at 800-982-6732 for recommended intervals, pricing and turn-around time for these services as well as for quotations on our standard products.

Continued product improvement necessitates that Endevco reserve the right to modify these specifications without notice. Endevco maintains a program of constant surveillance over all products to ensure a high level of reliability. This program includes attention to reliability factors during product design, the support of stringent Quality Control requirements, and compulsory corrective action procedures. These measures, together with conservative specifications have made the name Endevco synonymous with reliability.

ENDEVCO CORPORATION, 30700 RANCHO VIEJO ROAD, SAN JUAN CAPISTRANO, CA 92675 USA (800) 982-6732 (949) 493-8181 fax (949) 661-7231
www.endevco.com Email:applications@endevco.com

*obtained from www.endevco.com

Figure C.5 - Endevco model 136 voltage amplifier data sheet (page 2)

Low-Cost E Series Multifunction DAQ – 12 or 16-Bit, 200 kS/s, 16 Analog Inputs

NI E Series – Low-Cost

- 16 analog inputs at up to 200 kS/s, 12 or 16-bit resolution
- Up to 2 analog outputs at 10 kS/s, 12 or 16-bit resolution
- 8 digital I/O lines (TTL/CMOS); two 24-bit counter/timers
- Digital triggering
- 4 analog input signal ranges
- NI-DAQ driver that simplifies configuration and measurements

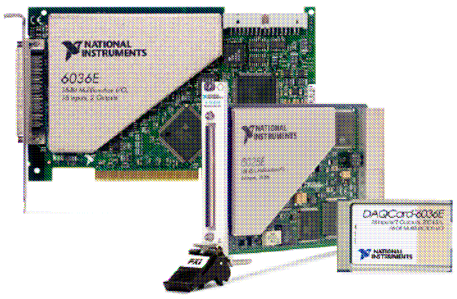
Families
- NI 6036E
- NI 6034E
- NI 6025E
- NI 6024E
- NI 6023E

Operating Systems
- Windows 2000/NT/XP
- Real-time performance with LabVIEW
- Others such as Linux® and Mac OS X

Recommended Software
- LabVIEW
- LabWindows/CVI
- Measurement Studio
- VI Logger

Other Compatible Software
- Visual Basic, C/C++, and C#

Driver Software (included)
- NI-DAQ 7



Family	Bus	Analog Inputs	Input Resolution	Max Sampling Rate	Input Range	Analog Outputs	Output Resolution	Output Rate	Output Range	Digital I/O	Counter/Timers	Triggers
NI 6036E	PCI, PCMCIA	16 SE/8 DI	16 bits	200 kS/s	±0.05 to ±10 V	2	16 bits	10 kS/s[1]	±10 V	8	2, 24-bit	Digital
NI 6034E	PCI	16 SE/8 DI	16 bits	200 kS/s	±0.05 to ±10 V	0	–	–	–	8	2, 24-bit	Digital
NI 6025E	PCI, PXI	16 SE/8 DI	12 bits	200 kS/s	±0.05 to ±10 V	2	12 bits	10 kS/s[1]	±10 V	8	2, 24-bit	Digital
NI 6024E	PCI, PCMCIA	16 SE/8 DI	12 bits	200 kS/s	±0.05 to ±10 V	2	12 bits	10 kS/s[1]	±10 V	8	2, 24-bit	Digital
NI 6023E	PCI	16 SE/8 DI	12 bits	200 kS/s	±0.05 to ±10 V	0	–	–	–	8	2, 24-bit	Digital

[1]10 kS/s typical when using the single DMA channel for analog output. 1 kS/s maximum when using the single DMA channel for either analog input or counter/timer operations. 1 kS/s maximum for PCMCIA DAQCard devices in all cases.

Table 1. Low-Cost E Series Model Guide

Overview and Applications

National Instruments low-cost E Series multifunction data acquisition devices provide full functionality at a price to meet the needs of the budget-conscious user. They are ideal for applications ranging from continuous high-speed data logging to control applications to high-voltage signal or sensor measurements when used with NI signal conditioning. Synchronize the operations of multiple devices using the RTSI bus or PXI trigger bus to easily integrate other hardware such as motion control and machine vision to create an entire measurement and control system.

Highly Accurate Hardware Design

NI low-cost E Series DAQ devices include the following features and technologies:

Temperature Drift Protection Circuitry – Designed with components that minimize the effect of temperature changes on measurements to less than 0.0010% of reading/°C.

Resolution-Improvement Technologies – Carefully designed noise floor maximizes the resolution.

Onboard Self-Calibration – Precise voltage reference included for calibration and measurement accuracy. Self-calibration is completely software controlled, with no potentiometers to adjust.

NI DAQ-STC – Timing and control ASIC designed to provide more flexibility, lower power consumption, and a higher immunity to noise and jitter than off-the-shelf counter/timer chips.

NI MITE – ASIC designed to optimize data transfer for multiple simultaneous operations using bus mastering with one DMA channel, interrupts, or programmed I/O.

NI PGIA – Measurement and instrument class amplifier that guarantees settling times at all gains. Typical commercial off-the-shelf amplifier components do not meet the settling time requirements for high-gain measurement applications.

PFI Lines – Eight programmable function input (PFI) lines that you can use for software-controlled routing of interboard and intraboard digital and timing signals.

RTSI or PXI Trigger Bus – Bus used to share timing and control signals between two or more PCI or PXI devices to synchronize operations.

RSE Mode – In addition to differential and nonreferenced single-ended modes, NI low-cost E Series devices offer the referenced single-ended (RSE) mode for use with floating-signal sources in applications with channel counts higher than eight.

Onboard Temperature Sensor – Included for monitoring the operating temperature of the device to ensure that it is operating within the specified range.

NATIONAL INSTRUMENTS

*obtained from www.ni.com

Figure C.6 - National Instruments 6024E data acquisition card data sheet (page 1)

Low-Cost E Series Multifunction DAQ – 12 or 16-Bit, 200 kS/s, 16 Analog Inputs

		Full-Featured E Series				Low-Cost E Series		Basic
Models		NI 6030E, NI 6031E, NI 6032E, NI 6033E	NI 6052E	NI 6070E, NI 6071E	NI 6040E	NI 6034E, NI 6036E	NI 6023E, NI 6024E, NI 6025E	PCI-6013, PCI-6014
Measurement Sensitivity[1] (mV)		0.0023	0.0025	0.009	0.008	0.0036	0.008	0.004
Nominal Range (V)								
Positive FS	**Negative FS**	**Absolute Accuracy (mV)**						
10	-10	1.147	4.747	14.369	15.373	7.560	16.504	8.984
5	-5	2.077	0.876	5.193	5.697	1.790	5.263	2.003
2.5	-2.5	–	1.190	3.605	3.859	–	–	–
2	-2	0.836	–	–	–	–	–	–
1	-1	0.422	0.479	1.452	1.556	–	–	–
0.5	-0.5	0.215	0.243	0.735	0.789	0.399	0.846	0.471
0.25	-0.25	–	0.137	0.379	0.405	–	–	–
0.2	-0.2	0.102	–	–	–	–	–	–
0.1	-0.1	0.061	0.064	0.163	0.176	–	–	–
0.05	-0.05	–	0.035	0.091	0.100	0.0611	0.106	0.069
10	0	0.976	1.232	6.765	7.269	–	–	–
5	0	1.992	2.119	5.391	5.645	–	–	–
2	0	0.802	0.850	2.167	2.271	–	–	–
1	0	0.405	0.428	1.092	1.146	–	–	–
0.5	0	0.207	0.242	0.558	0.583	–	–	–
0.2	0	0.098	0.111	0.235	0.247	–	–	–
0.1	0	0.059	0.059	0.127	0.135	–	–	–

Note: Accuracies are valid for measurements following an internal calibration. Measurement accuracies are listed for operational temperatures within ±1 °C of internal calibration temperature and ±10 °C of external or factory-calibration temperature. One-year calibration interval recommended. The Absolute Accuracy at Full Scale calculations were performed for a maximum range input voltage (for example, 10 V for the ±10 V range) after one year, assuming 100 pt averaging of data.
[1]Smallest detectable voltage change in the input signal at the smallest input range.

Table 2. E Series Analog Input Absolute Accuracy Specifications

		Full-Featured E Series				Low-Cost E Series		Basic
Models		NI 6030E, NI 6031E, NI 6032E, NI 6033E	NI 6052E	NI 6070E, NI 6071E	NI 6040E	NI 6034E, NI 6036E	NI 6023E, NI 6024E, NI 6025E	PCI-6013, PCI-6014
Nominal Range (V)								
Positive FS	**Negative FS**	**Absolute Accuracy (mV)**						
10	-10	1.430	1.405	8.127	8.127	2.417	8.127	3.835
10	0	1.201	1.176	5.685	5.685	–	–	–

Table 3. E Series Analog Output Absolute Accuracy Specifications

High-Performance, Easy-to-Use Driver Software

NI-DAQ is the robust driver software that makes it easy to access the functionality of your data acquisition hardware, whether you are a beginning or advanced user. Helpful features include:

Automatic Code Generation – DAQ Assistant is an interactive guide that steps you through configuring, testing, and programming measurement tasks and generates the necessary code automatically for NI LabVIEW, LabWindows/CVI, or Measurement Studio.

Cleaner Code Development – Basic and advanced software functions have been combined into one easy-to-use yet powerful set to help you build cleaner code and move from basic to advanced applications without replacing functions.

High-Performance Driver Engine – Software-timed single-point input (typically used in control loops) with NI-DAQ achieves rates of up to 50 kHz. NI-DAQ also delivers maximum I/O system throughput with a multithreaded driver.

Test Panels – With NI-DAQ, you can test all of your device functionality before you begin development.

Scaled Channels – Easily scale your voltage data into the proper engineering units using the NI-DAQ Measurement Ready virtual channels by choosing from a list of common sensors and signals or creating your own custom scale.

LabVIEW Integration – All NI-DAQ functions create the waveform data type, which carries acquired data and timing information directly into more than 400 LabVIEW built-in analysis routines for display of results in engineering units on a graph.

For information on applicable hardware for NI-DAQ 7, visit ni.com/dataacquisition.

Visit ni.com/oem for quantity discount information.

*obtained from www.ni.com

Figure C.7 - National Instruments 6024E data acquisition card data sheet (page 2)

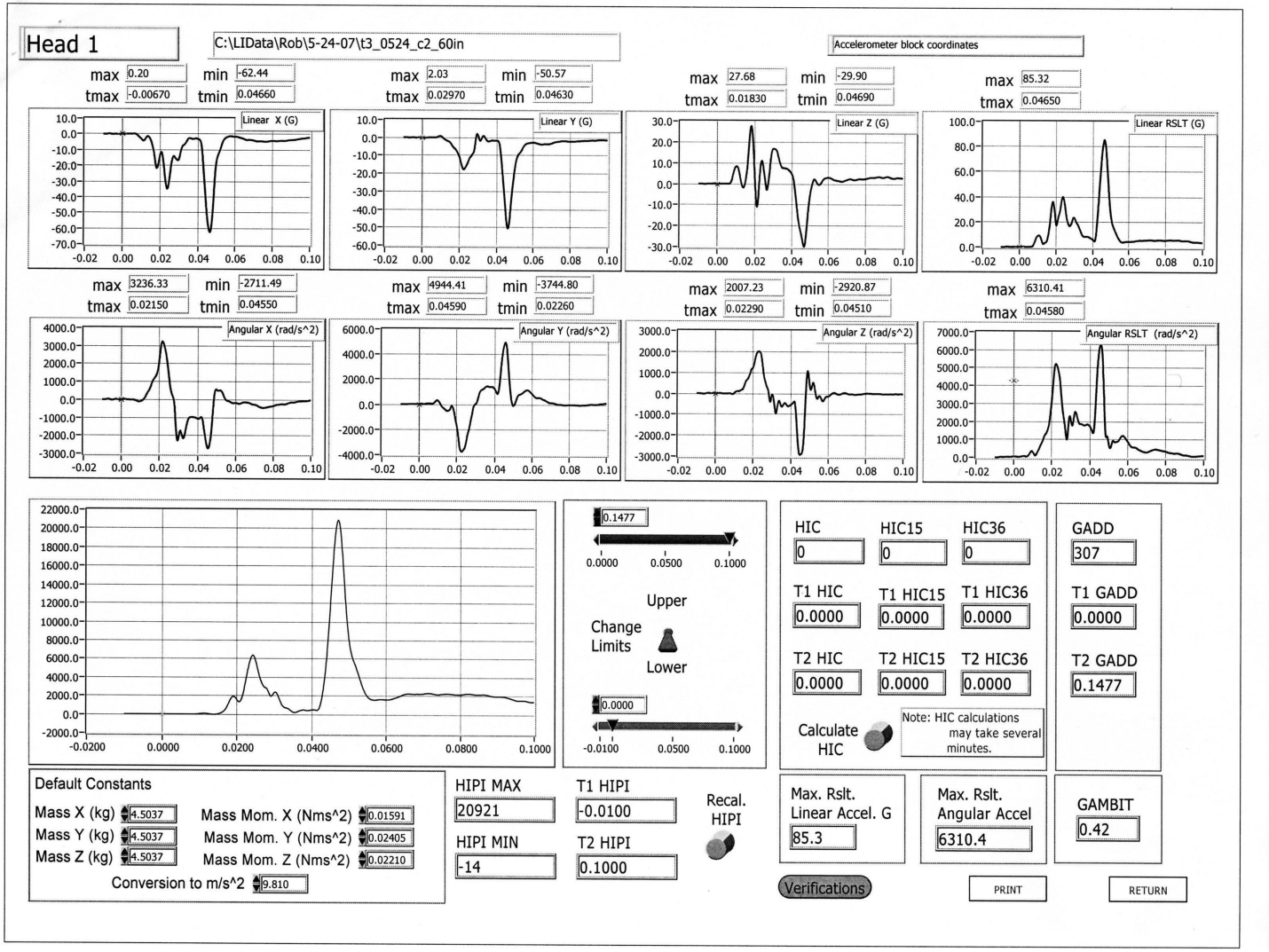


Figure C.8 - Sample of output screen from BIODAQ software

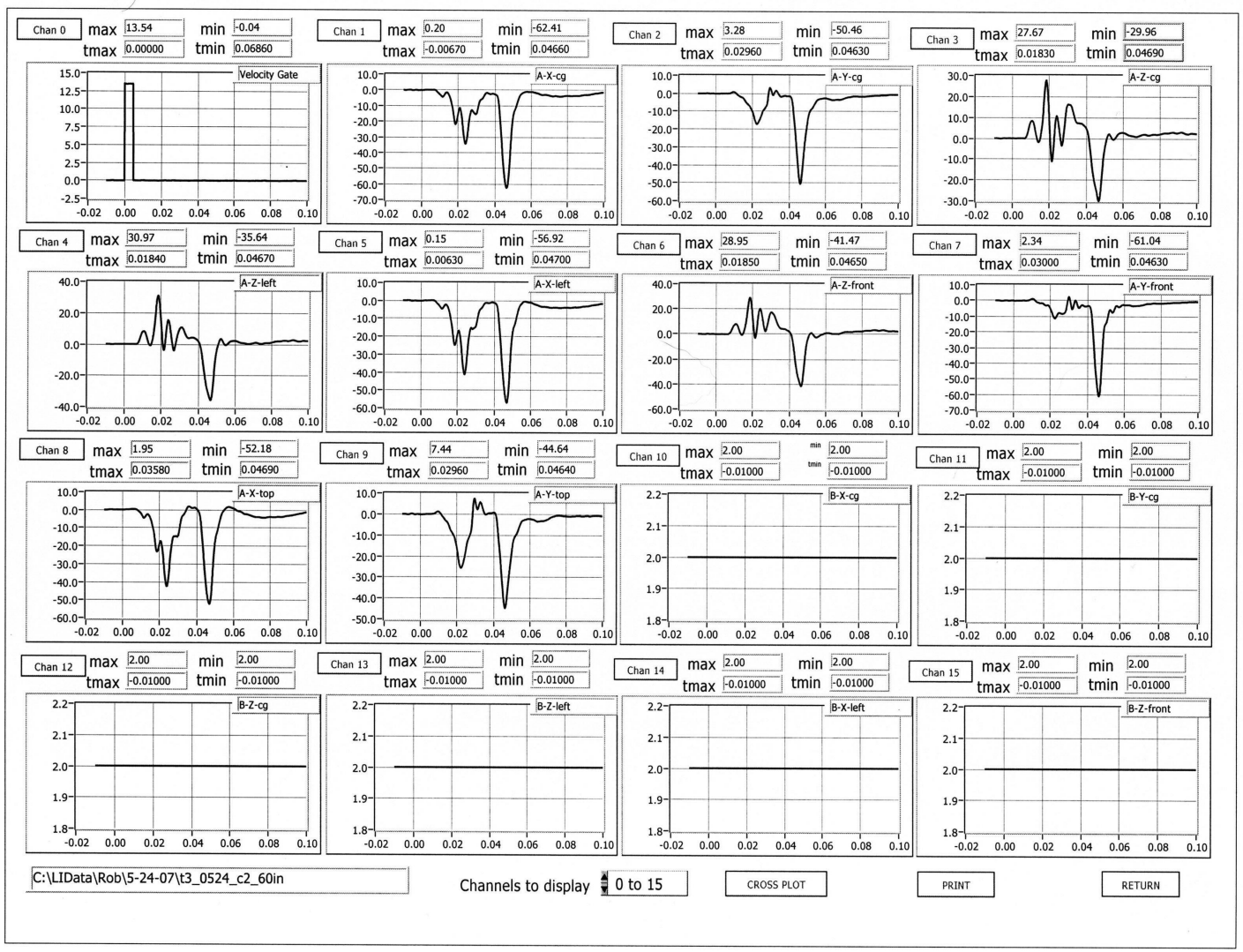


Figure C.9 - Sample of filtered data screen from BIODAQ software

VITA

Robert Paul Roy was born on March 13, 1981 in Oneida, Tennessee. He graduated as Valedictorian from Oneida High School in May of 1999. In the fall of 1999, he began his undergraduate education at the University of Tennessee, Knoxville. In May 2005, Robert graduated from UT with Bachelor of Science degrees in Aerospace and Mechanical Engineering. He began his graduate career in Fall 2005 and worked as a graduate teaching assistant for the Mechanical, Aerospace, and Biomedical Engineering at the University of Tennessee, Knoxville. He worked in the Sports Biomechanics Impact Laboratory on UT campus, and at Southern Impact Research Center in Rockford, TN during his undergraduate and graduate career. Robert graduated from UT with a Master's in Engineering Science in December 2007. He does not normally refer to himself in the third person.